Evaluation of iron sources in the Ross Sea

Elodie Salmon, Eileen E Hofmann, Michael S Dinniman, Walker O. Smith Jr

Evaluation of iron sources in the Ross Sea

Elodie Salmon, Eileen E. Hofmann, Michael S. Dinniman, Walker O. Smith

PII: S0924-7963(20)30125-1

DOI: https://doi.org/10.1016/j.jmarsys.2020.103429

Reference: MARSYS 103429

To appear in: *Journal of Marine Systems*

Received date: 8 December 2019

Revised date: 15 August 2020

Accepted date: 17 August 2020

Please cite this article as: E. Salmon, E.E. Hofmann, M.S. Dinniman, et al., Evaluation of iron sources in the Ross Sea, *Journal of Marine Systems* (2018), https://doi.org/10.1016/j.jmarsys.2020.103429

Evaluation of Iron Sources in the Ross Sea

Elodie Salmon[1, 2] (elodie.salmon@cnrs-orleans.fr , corresponding author)

Eileen E. Hofmann[1] (hofmann@ccpo.odu.edu)

Michael S. Dinniman[1] (msd@ccpo.odu.edu)

Walker O. Smith, Jr.[3,4] (wos@vims.edu)

[1]Center for Coastal Physical Oceanography, Old Dominion University, 4111 Monarch Way, Norfolk, VA 23508, USA

[2]Now at Laboratoire de Physique et Chimie de l'Environnement et de l'Espace, CNRS – Université Orléans – CNES (UMR 7328), 3A Avenue de la Recherche Scientifique, 45071 Orléans cedex 2, France.

[3]Virginia Institute of Marine Science, William & Mary, Gloucester Point, VA 23062, USA

[4]School of Oceanography, Shanghai Jiao Tong University, No.1954 Huashan Road, Xuhui Dist., Shanghai, PRC 2000230, China

Draft Date: août 19, 2020

Keywords: Ross Sea, dissolved iron sources, biogeochemical model, phytoplankton blooms, *Phaeocystis antarctica*.

Abstract

A one-dimensional numerical model that includes the complex life cycle of *Phaeocystis antarctica*, diatom growth, dissolved iron (dFe) and irradiance controls, and the taxa's response to changes in these variables is used to evaluate the role of different iron sources in supporting phytoplankton blooms in the Ross Sea. Simulations indicate that sea ice melt accounts for 20% of total dFe inputs during low light conditions early in the growing season (late November-early December), which enhances blooms of *P. antarctica* in early spring. Advective inputs of dFe (60% of total inputs) maintain the *P. antarctica* bloom through early January and support a diatom bloom later in the growing season (early to mid-January). In localized regions near banks shallower than 450 m, suspension of iron-rich sediments and entrainment into the upper layers contributes dFe that supports blooms. Seasonal dFe budgets constructed from the simulations show that diatom-associated dFe accounts for the largest biological reservoir of dFe. Sensitivity studies show that surface input of dFe from sea ice melt, a transient event early in the growing season, sets up the phytoplankton sequencing and bloom magnitude, suggesting that the productivity of the Ross Sea system is vulnerable to changes in the extent and magnitude of sea ice.

1. Introduction

Iron is central to growth and productivity of Antarctic waters, both in the deeper waters of the Antarctic Circumpolar Current and on continental shelves (Martin et al., 1990; Boyd et al., 2000; Coale et al., 2004, Marsay et al., 2017), similar to its role in other high nutrient, low chlorophyll regions (de Baar et al., 2005). Iron is supplied to Antarctic surface waters from atmospheric dust (Li et al., 2008; Tagliabue et al., 2009), sea ice ablation (Grotti et al., 2005; Lannuzel et al., 2010), glacial melt (Gerringa et al., 2012; Alderkamp et al., 2012; Sherrell et al., 2015), and vertical entrainment of deeper iron-rich waters (Marsay et al., 2014; McGillicuddy et al., 2015). Despite these potential pathways of supply, iron supply rates during the Antarctic spring/summer are low.

The primary productivity in the Ross Sea is estimated to be ca. 179 g C m^{-2} yr^{-1}, which is deemed to be the greatest biomass production of any coastal region in the Southern Ocean (Arrigo et al., 2008), and iron supply is critical in regulating phytoplankton growth, productivity and composition of this region (Smith et al., 2014). Atmospheric deposition rates of iron are low in the Ross Sea (Cassar et al., 2007), sea ice inputs are episodic, and vertical resupply is reduced by the stratification that persists throughout the growing season. The low supply rates lead to broad patterns of iron limitation, which have been confirmed by experimental manipulations (Sedwick et al., 2000; Olson et al., 2000; Feng et al., 2010) and field observations using iron-limitation proxies (Smith et al., 2011, 2013, Gerringa et al., 2015; Kustka et al., 2015; Hatta et al., 2017, Marsay et al. 2014, 2017).

Iron budgets constructed for the Ross Sea provide estimates of the relative importance of input pathways (McGillicuddy et al., 2015; Gerringa et al., 2015).

McGillicuddy et al. (2015) showed that sea ice melt and resupply from deep waters via sediment and Circumpolar Deep Water (CDW) account for most of the iron that supports primary production. Gerringa et al. (2015) found that dissolved iron supplied by sediments was the primary input supporting phytoplankton growth in early summer. The deep-water dissolved iron pathway was confirmed with tracer studies implemented with a high-resolution Ross Sea circulation model (Mack et al., 2017). Other studies showed that Modified Circumpolar Deep Water (MCDW), which is a colder and saltier version of CDW found on the Ross Sea continental shelf, and benthic sources provide dissolved iron that is important for supporting phytoplankton blooms (Kustka et al., 2015; Hatta et al., 2017). However, uncertainties remain about taxon-specific responses to iron additions, as well as spatial and temporal variations in supply and removal.

Phytoplankton assemblages in the Ross Sea are dominated by the haptophyte *Phaeocystis antarctica* and diatoms. Blooms of *P. antarctica* generally occur in austral spring, yet growth continues in parts of the Ross Sea throughout summer (Smith et al., 2014; Smith and Jones, 2015). Growth of the haptophyte in spring is facilitated by elevated iron concentrations and reduced irradiance imposed by ice, relatively deep vertical mixing, and low solar angles (Arrigo et al., 1999; Kroupenske et al., 2009). Conversely, diatoms grow in more stratified conditions, such as in areas with melting sea ice. Sedwick et al. (2011) showed that iron was reduced to low concentrations (ca. 0.06 nM) in spring by *P. antarctica* growth, and these concentrations persisted throughout the summer. Large diatom blooms observed in summer (Peloquin and Smith, 2007; Kaufman et al., 2014; Smith and Kaufman, 2018) are dependent on either new sources of

iron or greatly increased carbon/iron ratios under high light conditions. A direct comparison of iron strategies between diatoms and *P. antarctica* is unavailable.

The many environmental variables that are changing simultaneously (e.g., irradiance, iron concentrations, losses due to grazing and passive sinking, variable elemental ratios of plankton) make determining their interactions and controls on production via experimental manipulations challenging (Boyd et al., 2015). A taxon-specific numerical model provides one approach for assessing the role of irradiance and various pathways of iron supply in controlling biological production. Such models have proven to be powerful tools to understand the interactions among controlling variables and phytoplankton (e.g., Kaufman et al., 2017), and to begin to understand how regions will respond to future climate change. Models for *P. antarctica* have described its growth (e.g., Wang and Moore, 2011), and other models have focused on diatomaceous growth (e.g., Lancelot et al., 2000). Arrigo et al. (2003) assessed the temporal evolution of *P. antarctica* and diatom growth in different regions of the Ross Sea in response to the interactions of light and nutrients (NO_3 and iron). However, this model did not differentiate the two stages of *P. antarctica* life cycle. In this study a one-dimensional numerical model that includes the complexities of the *P. antarctica* life cycle, diatom growth, nitrate, iron, silicate and irradiance controls, and each taxa's response to the changes in these variables is implemented to evaluate the role of different iron sources and the two phytoplankton assemblages in primary production of the Ross Sea.

2. Methods

2.1 Model Overview

The biogeochemical model used in this study (Fig. 1) is based on Fiechter et al. (2009), with modifications appropriate for the Ross Sea. The model includes dynamics for the macronutrients nitrate-nitrogen (NO_3) and silicate (Si), and the micronutrient dissolved iron (dFe). Iron and silicate consist of dissolved and phytoplankton-associated components (Fe_p, Si_p), through inclusion of Fe:C and Si:C ratios, respectively. Primary producers are represented by diatoms and haptophytes, which are the bloom forming functional groups in the Ross Sea.

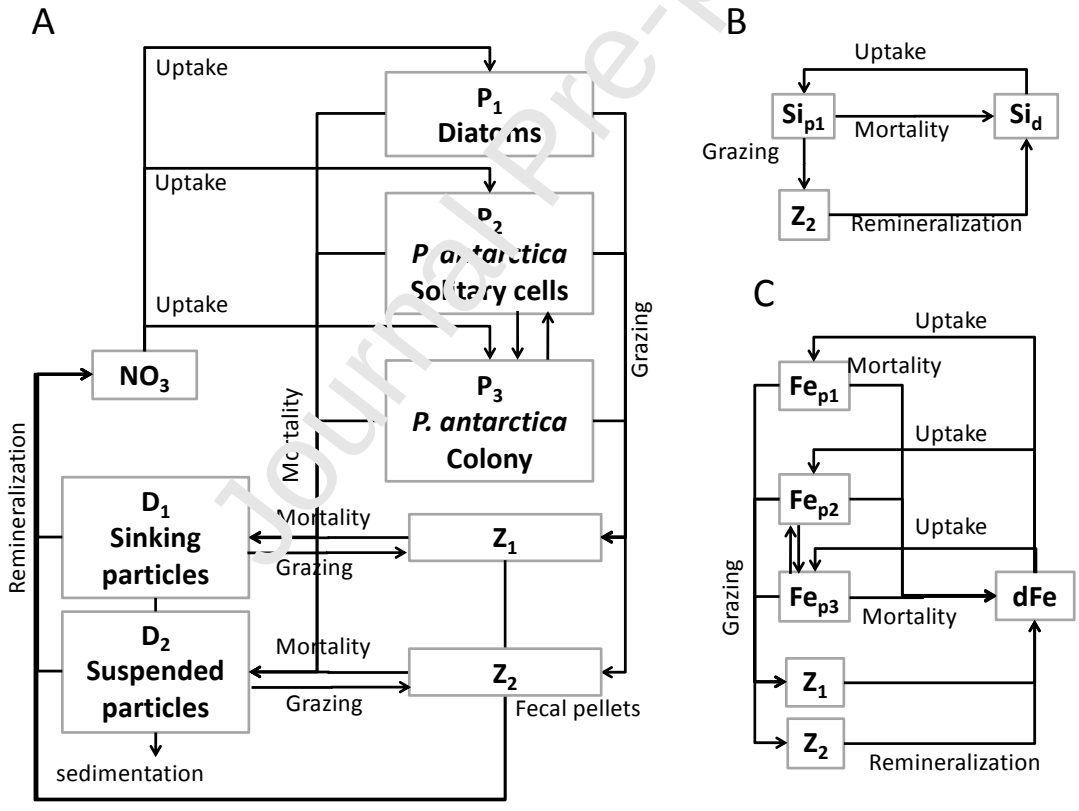

Figure 1: Schematic of the Ross Sea biogeochemical model dynamics for A) nitrate-nitrogen (NO_3), B), silicate (Si), and C) dissolved iron (dFe). Primary producers include diatoms (P_1) and *P. antarctica* solitary cells (P_2), and *P. antarctica* colonies (P_3). Grazers

include micro- (Z_1) and meso-zooplankton (Z_2) and detritus is separated into sinking (D_1) and suspended (D_2) particles. State variables are shown in the boxes; arrows represent the processes that affect changes in the state variables.

The diatom group (P_1, Fig. 1A) represents the dominant forms (*Fragilariopsis* spp., *Pseudonitzschia* spp.) found in blooms in the Ross Sea during summer (Smith et al., 2014). The haptophytes are represented by both phenotypes of *P. antarctica*, solitary cells and the colonial form (P_2 and P_3, respectively, Fig. 1A) that contribute to spring blooms in the Ross Sea (Smith et al., 2014). The two zooplankton groups represent mesozooplankton (Z_1, Fig. 1A) that grazes the three types of phytoplankton and microzooplankton (Z_2, Fig. 1A) that grazes exclusively on solitary cells of *P. antarctica*. Sinking and suspended particles are represented by two detrital components (D_1 and D_2, Fig. 1A). Zooplankton graze the detrital pool and a fraction of zooplankton fecal pellets is recycled to the nitrate (Powell et al., 2006).

Phytoplankton growth is supported by nitrate-nitrogen (NO_3, Fig. 1A) and dFe (Fig. 1C). Diatom growth is also dependent on the concentration of Si (Fig. 1B). The dFe pool receives inputs via remineralization of zooplankton fecal pellets and phytoplankton associated iron (Fe_p, Fig. 1C). Inputs to the Si pool are from remineralization of mesozooplankton fecal pellets and phytoplankton mortality (Fig. 1B). The model governing equations are nitrogen-based, except those that describe Si and dFe dynamics.

Equations and details specific to the Ross Sea implementation are given in the following sections. Details of the parameterizations used for the terms in the governing equations are provided in the supplementary information (Tables S1-S6).

2.2 Phytoplankton

2.2.1 Diatoms

The time (t) and vertical (z) dependence of diatoms is governed by

$$\frac{\partial P_1}{\partial t} = \mathrm{U_1P_1} - \mathrm{G_{11}Z_1} - \sigma_{d_1} P_1 + \omega_{P_1} \frac{\partial P_1}{\partial z} \quad (1)$$

where the terms represent light and nutrient-dependent growth, grazing removal by mesozooplankton, cell senescence, and vertical sinking, respectively. The two loss terms are dependent on the mortality rate, σ_{d1}, and the sinking rate, ω_{p1}, respectively. Values for these rate parameters as well as those used in the diatom nutrient and light parameterizations, described next, are given in Table S1.

Diatom growth is dependent on the concentrations of NO_3, dFe and Si, and light availability. Nutrient regulation of growth is determined by the minimum of the nitrate ($U_{(NO_3)_1}$), dFe ($U_{(dFe)_1}$) and Si ($U_{(SiO_4)_1}$) uptake rates as:

$$U_1 = \min(U_{(NO_3)_1}, U_{(dFe)_1}, U_{(SiO_4)_1}) \quad (2)$$

Nitrate uptake is assumed to follow a Michaelis-Menten formulation and is modified by irradiance (I) based on Platt et al. (1980) as:

$$U_{(NO_3)_1} = \frac{NO_3\, Vm_1}{NO_3 + k_{(NO_3)_1}} \left(1 - \exp(-\frac{\alpha_1 I}{Vm_1})\right) \exp(-\frac{\beta_1 I}{Vm_1}) \quad (3)$$

Irradiance is time (t) and vertically (z) dependent and is of the form:

$$I = I_0 \exp\left(k_z + k_{P_1} \int_z^0 P_1(z')dz' + k_{P_2} \int_z^0 P_2(z')dz' + k_{P_3} \int_z^0 P_3(z')dz'\right) \quad (4)$$

where the incident irradiance at the sea surface (I0) is attenuated by absorption by the water and the three phytoplankton groups (P1, P2, P3). Irradiance is proportionally reduced by the sea ice concentration fraction and is zero when sea ice totally covers the

sea surface. Irradiance rapidly increases as sea ice melts in the spring. In early spring in the Ross Sea, sea ice is removed from the shelf partially by off-shore winds creating ice-free regions where irradiance is suddenly available for primary production. However, the biogeochemical model represents a one-dimensional vertical water column in the central Ross Sea continental shelf and therefore does not allow the dynamics that produce this removal of sea ice (sea ice is only removed by in-situ melting) and increased irradiance.

Silicate uptake follows a Michaelis-Menten uptake of bio-available Si and is incorporated into the phytoplankton cells based on a local Si_p:C ratio:

$$U_{Si_{P_1}} = \frac{R_{Si_{P_1}}}{R_{Si_{P_1}} + k_{(Si_{P_1}:C)_1}} \quad (5)$$

where $R_{Si_{P1}}$ is the Si_p:C ratio in mmol Si (mol C)$^{-1}$ defined as:

$$R_{Si_{P_1}} = \frac{Si_{P_1}}{P_1(C/N)_1} \quad (6)$$

with Si_{P1} representing phytoplankton associated Si and $(C/N)_1$ is the diatom C:N molar ratio. The Si uptake rate is specified as a portion of the nitrate uptake rate by normalizing equation 5 by equation 3.

Similarly, iron uptake is based on the local Fe_p:C ratio of the bio-available iron incorporated in phytoplankton cells as:

$$U_{Fe_{P_1}} = \frac{(R_{Fe_{P_1}})^2}{\left(R_{Fe_{P_1}}\right)^2 + \left(k_{\left(Fe_{P_1}:C\right)_1}\right)^2} \quad (7)$$

where k is the local Fe_p:C ratio half saturation constant and $R_{Fe_{P1}}$ is the Fe_p:C ratio in μmol Fe (mol C)$^{-1}$ given by:

$$R_{Fe_{P_1}} = \frac{Fe_{P_1}}{P_1(C/N)_1} \quad (8)$$

where F_{p1} is the phytoplankton associated iron. The iron uptake rate is specified as a portion of the nitrate uptake rate by normalizing equation 7 by equation 3.

Mesozooplankton grazing rate is assumed to follow an Ivlev formulation (Ivlev, 1945) given by:

$$G_{11} = Rm_{11}(1 - \exp(-\Lambda_{11}P_1)) \quad (9)$$

where the Rm_{11} is the maximum ingestion rate and Λ_{11} is the Ivlev constant (Table S1).

2.2.2 *Phaeocystis antarctica*

P. antarctica occurs as solitary flagellated unicells or as colonies of non-flagellated cells that are embedded in a polysaccharide mucus (Smith et al., 2003). The relationship between environmental conditions and *P. antarctica* life cycle stage remains to be quantified, but inorganic nutrient limitation, especially dFe, grazing and irradiance may control morphotype selection in *Phaeocystis* spp. (Riegman et al., 1992; Riegman and van Boekel, 1996; Lancelot et al., 1998; Smith et al., 2003). Both morphotypes are implemented in this model.

The governing equation for *P. antarctica* solitary cells is given by:

$$\frac{\partial P_2}{\partial t} = \mathrm{U_2P_2} - \mathrm{G_{21}Z_1} - \mathrm{G_{22}Z_2} - \mathrm{f}_{cwm}\sigma_{d_3}P_3 - \sigma_{d_2}P_2 + \omega_{P_2}\frac{\partial P_2}{\partial z} \quad (10)$$

where the terms correspond to the growth of *P. antarctica* solitary cells (U_2), grazing by both meso- (G_{21}) and microzooplankton (G_{22}), transformation of *P. antarctica* colonial cells that become solitary cells ($f_{cwm}\sigma_{d3}$), senescence of *P. antarctica* solitary cells (σ_{d2}), and vertical sinking of solitary cells (ω_{p2}).

The nutrient uptake, light-limited growth, cell senescence, and vertical sinking parameterizations are of the same form as those used for diatoms, but with parameter

values that are appropriate for physiological responses of *P. antarctica* (Table S2). The growth rate of the two forms is controlled by the minimum of nitrate and iron availability as:

$$U_2 = \min(U_{(NO_3)_2}, U_{(dFe)_2}) \quad (11)$$

$$U_3 = \min(U_{(NO_3)_3}, U_{(dFe)_3}) \quad (12)$$

Losses of *P. antarctica* solitary cells from meso- and microzooplankton grazing are formulated as for diatoms with appropriate parameters values (Table S2).

The governing equation for *P. antarctica* colonies is given by

$$\frac{\partial P_3}{\partial t} = \mathrm{U_3P_3} - \mathrm{G_{31}Z_1} - \sigma_{d_3} P_3 + \omega_{P_3} \frac{\partial P_3}{\partial z} \quad (13)$$

where the terms correspond to growth, grazing loss to mesozooplankton, senescence of colonies, and the sinking of colonies, respectively. The parameterizations used for each term are similar to those used for equation (10), with appropriate parameter values (Table S2).

The *Phaeocystis* spp. morphotype selection is computed at each time step and is based on the relative proportions of the phytoplankton associated Fe_p:C ratio of the solitary (P_2) and colonial (P_3) forms of *P. antarctica* relative to an expected maximum intracellular Fe_p:C ratio, as:

$$\frac{\Delta \mathrm{P_2}}{\Delta t} = (1 - f_{sc2c})P_2 + f_{c2sc}P_3 \quad (14)$$

$$\frac{\Delta \mathrm{P_3}}{\Delta t} = f_{sc2c}\, P_2 + (1 - f_{c2sc})P_3 \quad (15)$$

which accounts for the addition of solitary cells from colonies (f_{c2sc}) and of flagellate cells to colonies (f_{sc2c}).

The fraction of the solitary cells that change to the colonial morphotype (f_{sc2c}) is given by:

$$f_{sc2c} = \frac{Fe_{P_2}}{P_2(C/N)_2}\left(\frac{C}{Fe}\right)_{max} \quad (16)$$

and the fraction of *P. antarctica* cells living in colonies that become solitary cells (f_{c2sc}) is given by:

$$f_{c2sc} = max_{c2sc}\frac{Fe_{P_3}}{f_{cwm}P_3(C/N)_3}\left(\frac{C}{Fe}\right)_{max} \quad (17)$$

where max_{c2sc} is 0.25, which is the maximum fraction of cells living in colonies that become flagellate cells (Shields and Smith, 2009). This fraction includes only the colonial cells not bound by mucous (*fcwm*).

2.3 Nitrate and Silicate

The time (*t*) and vertical (*z*) dependence of nitrate-nitrogen is governed by:

$$\frac{\partial NO_3}{\partial t} = -U_1P_1 - U_2P_2 - U_3P_3$$
$$+\nu_{n_{11}}G_{11}Z_1 + \nu_{n_{21}}G_{21}Z_1 + \nu_{n_{31}}G_{31}Z_1 + \nu_{n_{22}}G_{22}Z_2$$
$$+\nu_{n_{d11}}G_{d11}Z_1 + \nu_{n_{d22}}G_{22}Z_2$$
$$+\delta_1D_1 + \delta_2D_2 \quad (18)$$

where the terms represent uptake of nitrate by all three phytoplankton types, recycling via mesozooplankton grazing on the three phytoplankton groups, recycling via microzooplankton grazing on solitary cells, recycling via zooplankton grazing on detritus, and remineralization from the two detrital pools. The portion of zooplankton fecal pellets that is returned to the nitrate pool is given by ν_n (Powell et al., 2006). The grazing formulations are defined as in section 2.2.1 and parameter values are given in Table S3.

Dissolved Si dynamics are given by:

$$\frac{\partial SiO_4}{\partial t} = -U_1Si_{P_1} + f_{Si_{rem}}G_{11}Z_1\frac{Si_{P_1}}{P_1} + f_{Si_{rem}}\sigma_{d_1}Si_{P_1} \quad (19)$$

where the terms represent removal by diatom uptake, remineralization from zooplankton grazing and cell senescence, respectively. The terms in equation (19) depend on the ratio of Si incorporated into diatoms (Si_{p1}) and phytoplankton carbon content (P_1 is converted from mmol N m^{-3} to mol C m^{-3}), rather than the local concentration of Si, following the approach proposed by Fietcher et al. (2009).

Diatom-associated Si is given by:

$$\frac{\partial Si_{P_1}}{\partial t} = U_1 Si_{P_1} - G_{11} Z_1 \frac{Si_{P_1}}{P_1} - \sigma_{d_1} Si_{P_1} \quad (20)$$

where the terms correspond to the portion of Si uptake by diatoms that is incorporated into the biomass (U_1), and loss of phytoplankton-associated Si through remineralization by grazing (G_{11}) and senescence (σ_{d1}). Parameter values used for the Si parameterizations are given in Table S4.

2.4 Dissolved Iron

The dFe is dependent on the processes included in the governing equations for each phytoplankton group (Fe_{p1}, Fe_{p2} and Fe_{p3}) as:

$$\frac{\partial dFe}{\partial t} = -U_1 dFe - U_2 dFe - U_3 dFe$$
$$+ f_{rem} Fe_{P_1} \sigma_{d_1} \frac{G_{d_{11}} Z_1}{D_1} + f_{rem}\left(Fe_{P_2}\sigma_{d_2} + (1 - f_{cwm}) Fe_{P_3}\sigma_{d_3}\right)\frac{G_{d_{22}} Z_2}{D_2}$$
$$+ f_{rem} G_{11} Z_1 \frac{Fe_{P_1}}{P_1} + f_{rem} G_{21} Z_1 \frac{Fe_{P_2}}{P_2} + f_{rem} G_{31} Z_1 \frac{Fe_{P_3}}{P_3} + f_{rem} G_{22} Z_2 \frac{Fe_{P_2}}{P_2}$$
$$+ f_{rem}\sigma_{d_1} Fe_{P_1} + f_{rem}\sigma_{d_2} Fe_{P_2} + (1 - f_{cwm})\sigma_{d_3} Fe_{P_3} \quad (21)$$

where the first five terms represent removal by the three phytoplankton groups, and remineralization of Fe_p (f_{rem}) via degradation of detrital material produced from senescence of diatoms (σ_{d1}), solitary cells (σ_{d2}), and colonies ($(1\text{-}f_{cwm})\sigma_{d3}$) expressed in

terms of zooplankton grazing (Z_1, Z_2) on the two detrital pools, respectively. The next four terms represent Fe_p remineralized (f_{rem}) from mesozooplankton grazing on diatoms ($G_{11}Z_1$), *P. antarctica* solitary cells ($G_{21}Z_1$) and colonies ($G_{31}Z_1$), and microzooplankton grazing on *P. antarctica* solitary cells ($G_{22}Z_2$), respectively. This remineralization is dependent on the carbon content of each group (P_1, P_2 and P_3 in mol C m^{-3}). The final three terms represent direct Fe_p remineralization from diatom (σ_{d1}), *P. antarctica* solitary cells (σ_{d2}) and colony (σ_{d3}) senescence. The remineralization rate of Fe_p is assumed to be the same for the different remineralization processes.

Incorporation of dFe into diatoms cells is governed by:

$$\frac{\partial Fe_{P_1}}{\partial t} = U_1 Fe_{P_1} - G_{11} Z_1 \frac{Fe_{P_1}}{P_1} - \sigma_{d_1} Fe_{P_1} \quad (22)$$

which is determined by nutrient and light limited uptake rate (U_1), loss by mesozooplankton grazing ($G_{11}Z_1$), and loss by cell senescence respectively.

The dFe-mediated selection of the two *Phaeocystis* spp. morphotypes is given by equations 14 to 17. The dFe associated with solitary *P. antarctica* cells (Fe_{p2}) is governed by:

$$\frac{\partial Fe_{P_2}}{\partial t} = U_2 Fe_{P_2} - f_{cwm} \sigma_{d_3} Fe_{P_3} - G_{21} Z_1 \frac{Fe_{P_2}}{P_2} - G_{22} Z_2 \frac{Fe_{P_2}}{P_2} - \sigma_{d_2} Fe_{P_2} \quad (23)$$

where the terms correspond to uptake and transition of cells from colony to solitary stage because of colony senescence ($f_{cwm}\sigma_{d3}$). Loss of Fe_p is through grazing by meso- and microzooplankton, $G_{21}Z_1$ and $G_{22}Z_2$ and senescence of solitary cells (σ_{d2}), respectively.

Similarly, dFe associated with *P. antarctica* colonies (dFe_{p3}) is governed by:

$$\frac{\partial Fe_{P_3}}{\partial t} = U_3 Fe_{P_3} - G_{31} Z_1 \frac{Fe_{P_3}}{P_3} - \sigma_{d_3} Fe_{P_3} \quad (24)$$

where the terms represent uptake by colonial cells (1-f_{c2sc}), loss by grazing by mesozooplankton ($G_{31}Z_1$) and by senescence (σ_{d3}), respectively. Parameter values are given in Table S5.

2.5 Zooplankton

The time-dependent changes in mesozooplankton concentration are governed by:

$$\frac{\partial Z_1}{\partial t} = \left(1 - \nu_{n_{11}}\right)G_{11}Z_1 + \left(1 - \nu_{n_{21}}\right)G_{21}Z_1 + \left(1 - \nu_{n_{31}}\right)G_{31}Z_1 + \left(1 - \nu_{n_{d11}}\right)G_{d11}Z_1 - \zeta_1 Z_1 \quad (25)$$

where the first four terms correspond to gains from grazing on diatoms (G_{11}, ν_{n11}), *P. antarctica* solitary cells (G_{21}, ν_{n21}) and colonies (G_{31}, ν_{n31}) and large detritus (G_{d11}, ν_{d11}), respectively (Powell et al., 2006). A fraction (ν) of the zooplankton fecal pellets is directly remineralized to the nitrate pool. Loss by mortality of mesozooplankton (ζ_1) is transferred to the large particle detrital pool.

Time-dependent changes in microzooplankton are governed by:

$$\frac{\partial Z_2}{\partial t} = \left(1 - \nu_{n_{22}}\right)G_{22}Z_2 + \left(1 - \nu_{n_{d22}}\right)G_{d22}Z_2 - \zeta_2 Z_2 \quad (26)$$

where the first two terms represent gains from grazing on *P. antarctica* solitary cells and suspended detritus, respectively (Powell et al., 2006). A fraction (ν_{d22}) of the grazed material is remineralized to the nitrate pool and losses from mortality (ζ_2) are transferred to the suspended detrital pool. Parameter values are given in Table S6.

2.6 Detritus

The large detritus pool is described by the governing equation:

$$\frac{\partial D_1}{\partial t} = \sigma_{d_1} P_1 + \zeta_1 Z_1 - \delta_1 D_1 - G_{d11} Z_1 + \omega_{d_1} \frac{\partial D_1}{\partial z} \quad (27)$$

where the first four terms correspond to gains from diatom senescence (σ_{d1}) and mesozooplankton mortality (ζ_1), and losses from remineralization (δ_1) and degradation of the detritus (G_{d11}), respectively. The final term represents vertical sinking of the particles (ω_{d1}).

The governing equation for the smaller suspended detritus pool is given by:

$$\frac{\partial D_2}{\partial t} = \sigma_{d_2} P_2 + (1 - f_{cwm})\sigma_{d_3} P_3 + \zeta_2 Z_2 - \delta_2 D_2 - G_{d22} Z_2 + \omega_{d_2} \frac{\partial D_2}{\partial z} \quad (28)$$

where the first three terms are gains from *P. antarctica* solitary cells senescence (σ_{d2}), the disposal of colonial mucus ($(1-f_{cwm})\sigma_{d3}$), and microzooplankton mortality (ζ_2), respectively. Losses are from remineralization (δ_2) and degradation (G_{d22}). The final term is sinking of the suspended particles (ω_{d2}). Parameter values used for the detritus equations are given in Table S6.

2.7 Model Implementation

The time-dependent biogeochemical model was implemented with a version of the Regional Ocean Modeling System (Haidvogel et al., 2008) that used an idealized periodic domain with a 6x6 horizontal grid, with horizontal spacing of 9 km. The model domain represents a general site in the central Ross Sea continental shelf that is removed from influences of land and the Ross Ice Shelf. The vertical dimension has 32 grid points between the surface and 622 m, with variable spacing (i.e., 5.5-6 m near the surface and

40 m at bottom). The model domain has periodic lateral boundaries in both directions.

The initial conditions for the circulation model were taken from vertical salinity and potential temperature profiles obtained from a three-dimensional Ross Sea circulation model (Dinniman et al. 2011). Sea ice was simulated with a dynamic sea ice model (Budgell, 2005) as described in Dinniman et al. (2015). Total shortwave radiation was calculated analytically (Zillman, 1972) based on latitude/longitude, time of day, clouds (Laevastu, 1960; analytically set to 0.6), air temperature and humidity. Other atmospheric forcing was computed using the COARE 3.0 bulk flux algorithm (Fairall et al., 2003) to compute fluxes from imposed atmospheric values (Table S7).

The biogeochemical simulations span the entire growing season (early November to late March), which includes the retreat and advance of the seasonal ice and polynya formation. However, simulating the seasonal sea ice cycle and opening and closing of polynyas in a doubly periodic domain is not possible because of the inability to correctly represent ice divergence. Therefore, the timing of the seasonal sea ice cycle is determined by imposing wind speed and air temperature conditions that allow the ice concentration and thickness to change as a result of thermodynamic processes. This approach produces air temperatures that are too warm in the summer and too cold in the winter relative to observed conditions, but allowed for the proper seasonal ice cycle (including brine rejection) and the formation of deep winter mixed layers that match observed conditions over the Ross Sea continental shelf (i.e., Gordon et al., 2000, Piñones et al., 2019).

2.8 Simulation design

The biogeochemical simulations are designed to evaluate the relative contributions of different dFe sources and concentrations to the development of phytoplankton blooms and the relative abundance of the haptophyte, *P. antarctica* and diatoms in the Ross Sea (Table 1). The base case simulation includes a variable sea ice cover, and dFe inputs from melting sea ice, mid-water supply (MW), which is derived from lateral inputs and deep dFe rich water, and sediment resuspension; all identified as possible contributors to the Ross Sea iron budget (McGillicuddy et al., 2015; Gerringa et al., 2015; Kustka et al., 2015; Hatta et al., 2017; Mack et al., 2017; Marsay et al., 2014, 2017). The three dFe sources are implemented using a relaxation scheme that is applied over variable depth and time scales. The maximum dFe concentration and the time scale for the relaxation scheme are set for each simulation. Changes to dFe concentrations in water masses that originate off-shelf (i.e., CDW) and are then modified on the shelf due to circulation around shallow banks in the Ross Sea are not resolved by the idealized model domain. Rather, the relaxation scheme serves to maintain a desired dFe concentration for a given depth.

Inputs of dFe from sea ice ablation are variable and are specified with a time-dependent relationship that relaxes to a maximum iron concentration (dFe_{Max}) over a specified time scale (t_{Fe}) as:

$$dFe_{MaxVar} = t_{Fe}\, t_{doy}\, dFe_{Max}\, exp\left(1 - t_{doy}\, dFe_{Max}\right) \quad (29)$$

where t_{Fe} was set to 0.2 day, t_{doy} is the day of the year, and dFe_{Max} was set to 0.2 nM. The time scale (t_{Fe}) and the maximum dFe concentration (dFe_{Max}) values used for the simulations are based on observations of dFe release and sea ice melt (Lannuzel et al.,

2010). The maximum concentration of dFe released into the surface water occurs at the beginning of the growing season and slows in summer. The sea ice dFe input function was implemented between December 15 and January 15, which corresponds to the timing of sea ice melt in the Ross Sea (Jacobs and Comiso, 1989). The vertical extent of the effect of this dFe supply was tested for depths between the surface and 30 m (Table 1), which consider the effects of stratification and/or mixed layer depth on limiting the influence of dFe input from sea ice melt.

Table 1: Summary of Ross Sea biogeochemical model simulations. The simulations are designed to evaluate the dissolved iron (dFe) inputs provided by melting sea ice, mid-water input (MW) and sediment resuspension on *P. antarctica* and diatom growth. The dFe source, concentration (nM), depth of influence (m), and time scale of input (per day) are given for each simulation. The dFe concentration from sea ice (dFe_{MaxVar}) varies with time following equation 29. Multiple depths of influence are denoted by parentheses. Simulations included sea ice cover, except as noted. Specifics of individual simulations are provided in the text.

Simulation	Dissolved iron (dFe) source inputs			
	Sea ice present	Sea ice	MW	Sediment
		nM, m, d	nM, m, d	nM, m, d
Base case	Yes	dFe_{MaxVar}, 10, 0.2	0.2, 100, 90	0.6, 550, 120
Sea ice	Yes	dFe_{MaxVar}, (1, 10, 30), 0.2	-	-
Sea ice	No	dFe_{MaxVar}, 10, 0.2		
MWV	Yes	-	0.2, 100, (5, 90)	-
MWV	No	-	0.2, 100, 90	-
Sediment	Yes	-	-	0.6, (550, 300), 120
Sediment	No	-	-	0.6, (550, 300), 120

The mid-water inputs (MW) of dFe represent contributions from unspecified water column sources that include lateral inputs from mesoscale eddies and/or MCDW, which is the water mass over the continental shelf that comes onto the shelf at mid-depths as CDW and then modified by local processes (Jacobs and Giulivi, 1999). Field observations indicate that the mean dFe concentration of deep dFe rich water is about 0.2 nM (McGillicuddy et al., 2015; Mack et al., 2017, Gerringa et al., 2015; Kustka et al., 2015; Hatta et al., 2017, Marsay et al. 2014 and 2017). This MWV input was included by relaxing between the surface and 100 m a concentration of 0.2 nM over variable time scales (5 to 90 days, Table 1). The effect of sea ice on modifying the MWV input of dFe was evaluated with simulations with and without sea ice cover (Table 1).

The input of dFe from sediment resuspension from shallow banks in the Ross Sea is simulated by increasing the dFe concentration in the model layer closest to the bottom. This increase is relaxed to a dFe concentration of 0.6 nM (Marsay et al., 2014) with a 120-day time scale from the bottom of the water column at 622 m to minimum depths of 300 and 550 m (Table 1). The influence of sea ice cover on the vertical transport of this dFe supply was also evaluated (Table 1).

Initial conditions for NO_3 and Si were set to 30 and 82 mM, respectively, based on observations made in the western central Ross Sea (McGillicuddy et al. 2015; Smith and Kaufman, 2018). The NO_3 concentration in the upper 50 m was relaxed to a concentration of 22 μM with a 5-day time scale. The Si concentration was relaxed to a value of 65 μM in the upper 100 m with a 90-day time scale. These inputs represent the effect of mesoscale and higher frequency inputs, which are not resolved in the one-dimensional implementation of the biogeochemical model. The initial dFe concentration

was set to 0.1 nM, which corresponds to observed average concentrations in the Ross Sea (Sedwick et al. 2011; Marsay et al. 2014). The depths and frequency of dFe inputs from the different sources are given in Table 1. All simulations were initialized on 1 January and run for 4 years to assure model stabilization. The results from October of year 3 to April of year 4 of each simulation were used for the analyses.

3. Model results

3.1 Base case simulation

The base case simulation provides calibration and verification of the biogeochemical model using observations from a high primary production region of the Ross Sea (Smith et al., 2011). The simulated vertical distribution of nitrate, averaged over the simulation, shows the expected increase in concentration with depth (Fig. 2A). Nitrate concentrations in the upper 200 m range between 17 and 32 µM, which agree with observations. The simulated vertical profiles of dissolved Si and biogenic Si (Fig. 2B, C) increase and decrease with depth, respectively. The simulated Si concentrations range from 60 to 83 µM in the upper 200 m, which match observed concentrations (Fig. 2B). Simulated biogenic Si concentrations between the surface and 80 m match observed values (Fig. 2C), but below 100 m the values are lower than those observed.

The simulated average vertical distribution of dFe concentration increases from 0 at the surface to 0.1 nM at 100 m and to about 0.6 nM at 600 m (Fig. 2D, supplementary document C, Figure SC32). The simulated dFe profile falls within the range of observed dissolved iron concentrations in the Ross Sea (McGillicuddy et al., 2015; Mack et al. 2017), and is consistent with other measurements of dFe concentration (Sedwick et al.

2011; Gerringa et al., 2015; Kustka et al., 2015; Hatta et al., 2017; Marsay et al., 2014 and 2017).

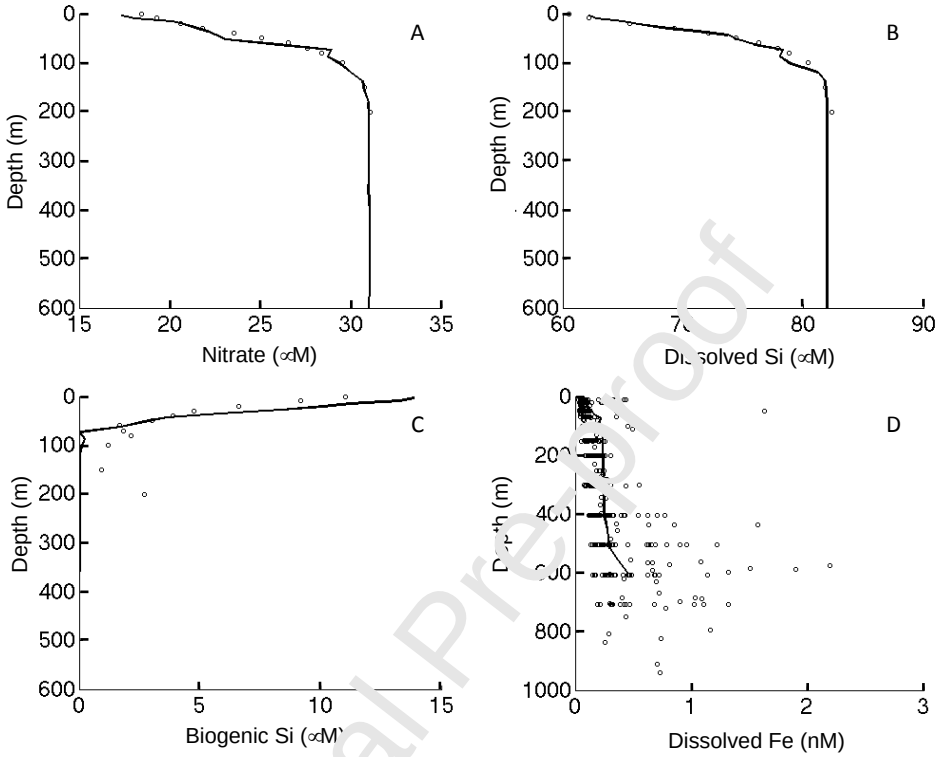

Figure 2: Simulated vertical profiles averaged over a growing season (solid line) of A) nitrate, B) dissolved silicate, C) biogenic silica, and D) dissolved iron. Observed nutrient concentrations (circles) were obtained as part of a Ross Sea field program that occurred in January-February 2012 (McGillicuddy et al., 2015).

The simulated time evolution of phytoplankton shows a bloom of *P. antarctica* colonies (PA_c, Fig.3A) that begins coincident with sea ice removal in late November-early December, reaches a maximum in mid-December, declines beginning in early January, and ends in early February. Solitary cells show a similar pattern but with a smaller biomass (PA_sc, Fig. 3A). The blooms of *P. antarctica* solitary cells and colonies

are underestimated in October-early November because of the inability to simulate the sudden high irradiance that occurs as a result of rapid rate of sea ice removal. The peak of the *P. antarctica* bloom is followed by a diatom bloom that starts growing late November, and reaches its maximum concentration in early January (Fig. 3A). The observed surface chlorophyll over the growing season increases in early December and shows a second increase in early to mid-January (Fig. 3A). The progression of the simulated haptophyte bloom to a diatom bloom is consistent with this observed pattern (Fig. 3A) and with the conceptual representation of the temporal phytoplankton composition in the Ross Sea proposed by Smith et al. (2014). The progression of the simulated depth-integrated chlorophyll shows general agreement with observations (Fig. 3B). The simulated surface chlorophyll production associated with diatoms is 3.7 mg m^{-3}, and that for *P. antarctica* is 11.1 mg m^{-3}. The simulated seasonal depth-integrated chlorophyll production for diatoms and *P. antarctica* are respectively, 78.3 and 171.0 mg m^{-2}.

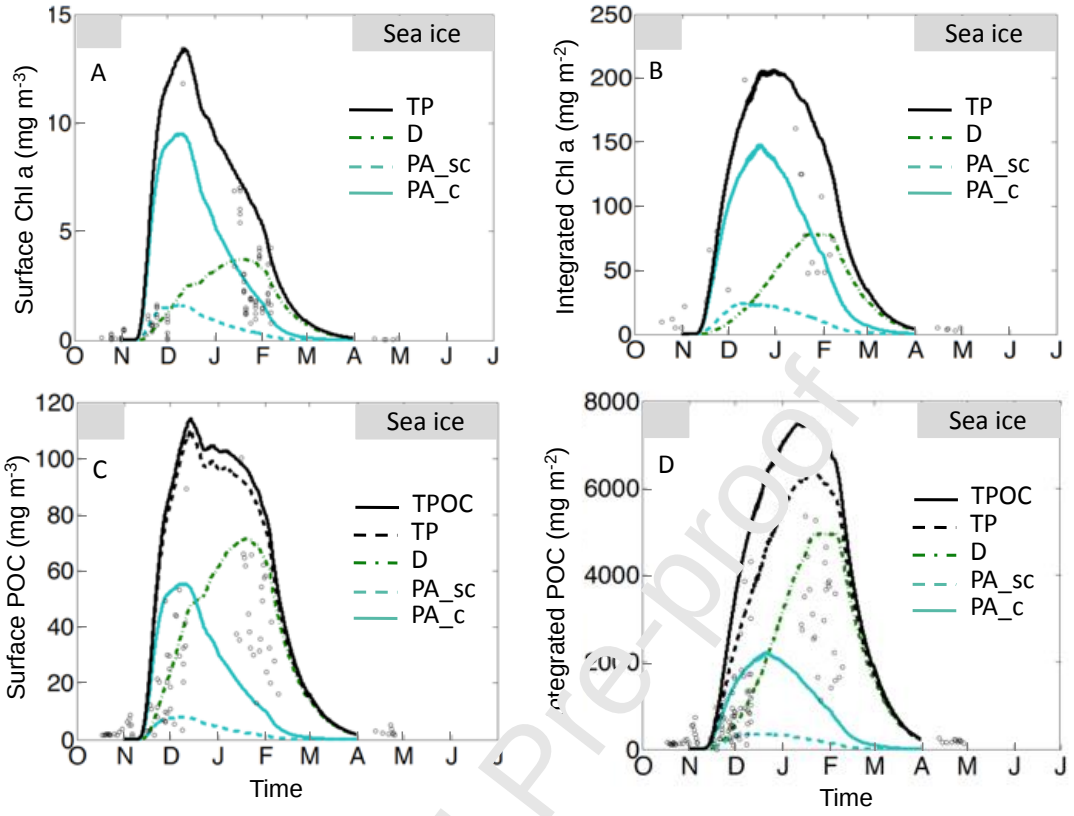

Figure 3: Simulated time evolution of A) surface and B) depth-integrated chlorophyll (Chl a) obtained for total phytoplankton (TP, black dashed line), diatoms (D, green dash-dot line), *P. antarctica* solitary cells (PA_sc, cyan dashed line) and *P. antarctica* colonies (PA_c, cyan solid line). Simulated time evolution of C) surface and D) depth-integrated particulate organic carbon (POC) based on total phytoplankton and detritus (TPOC, black solid line), total phytoplankton (TP, black dashed line), diatoms (D, green dash-dot line), *P. antarctica* solitary cells (PA_sc, cyan dashed line) and *P. antarctica* colonies (PA_c, cyan solid line). Observed POC values (circles in A, B, C and D) are from field measurements made in the Ross Sea (Smith et al., 2000). Depth-integrated values are from the surface to 80 m which corresponds to 1% surface irradiance level. The presence of simulated sea ice is indicated (grey shading).

The magnitude and timing of the simulated surface and integrated particulate organic carbon (POC) are consistent with observations (Fig. 3C, D). However, the POC associated with the *P. antarctica* colony bloom early in the growing season is smaller than that associated with the diatom bloom later in the growing season. This pattern is consistent with the seasonal surface POC production associated with the simulated *P. antarctica* (solitary cells and colonies) and diatoms, which are 63.3 and 71.6 mmol m^{-3}, respectively. The simulated depth-integrated seasonal POC production is higher for diatoms than for *P. antarctica*, 4,980 versus 2,550 mmol m^{-2}, respectively. These trends are reversed when carbon content is converted to chlorophyll.

Seasonal nitrogen, silicate and dFe budgets were constructed for each simulation based on values integrated over 80 m and accumulated over the growing season from 1 November through 31 March of the following year (see supplementary document-B). The seasonal nitrogen budget constructed from the base case simulation (Fig. 4A) shows that the nitrogen associated with *P. antarctica* colonies (78 mmol m^{-2}) and solitary cells (15 mmol m^{-2}) is about 36% and 7%, respectively, of that associated with diatoms (216 mmol m^{-2}). Sinking and suspended particles are respectively 2% and 21% of the diatom nitrogen. The nitrogen associated with grazers (Z_1 and Z_2) is minimal. The largest transfer from the nitrogen reservoir is through uptake by diatoms (56 μmol N m^{-2}); transfer to *P. antarctica* solitary cells and colonies is about 18% of this value. Senescence of *P. antarctica* solitary cells, which are released as colonies disintegrate, is the largest removal of nitrogen (400 μmol m^{-2}). The nitrogen associated with the mucus released as

the colonies disintegrate (69 μmol N m^{-2}) and that from solitary cell senescence provide more than half of the inputs to the suspended particulate nitrogen pool (Fig. 4A).

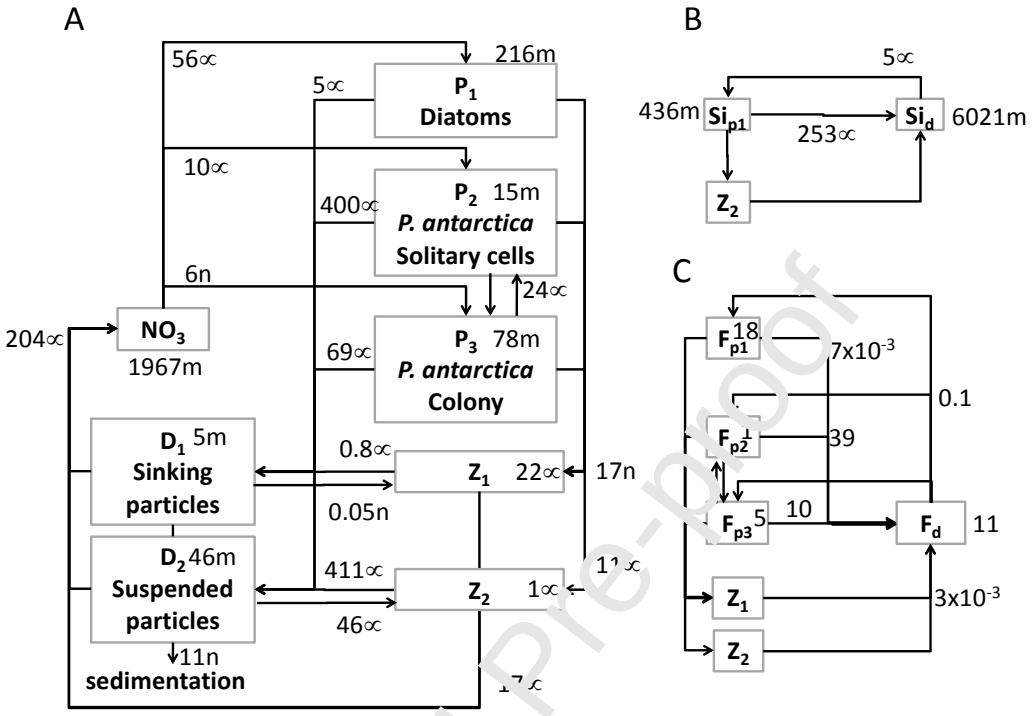

Figure 4: Seasonal budgets for A) nitrate-nitrogen, B) silicate, and C) dissolved iron (dFe) constructed from the Ross Sea base case simulation. Values shown for the state variables represent the contributions of each to the total nutrient pool. Values on the arrows indicate the transfer between pools. Only significant values for the nutrient pools are shown, which are defined as >1 mmol N m^{-2}, >0.5 mmol SiO_4 m^{-2}, and >1 nmol dFe m^{-2}. The values for transfers between pools are given as: m-millimoles (10^{-3}), μ-micromoles (10^{-6}), n-nanomoles (10^{-9}).

The Si associated with diatoms is about 7% of the total Si reservoir (6,020 mmol Si m^{-2}, Fig. 4B). Uptake by diatoms is the primary transfer from this reservoir. Transfers into the reservoir are by remineralization and diatom mortality. The diatom-associated

iron (Fe_{p1}) represents the largest reservoir (18 nmol Fe m^{-2}) in the seasonal dFe budget (Fig. 4C). The dFe reservoir (11 nmol dFe m^{-2}) exceeds the total dFe associated with *P. antarctica* colonies and solitary cells, 5 and 1 nmol Fe m^{-2}, respectively. Transfers from the dFe reservoir are by phytoplankton uptake, with the largest removal by *P. antarctica* solitary cells (0.1 nmol Fe m^{-2}). Diatom mortality provides the largest input to the dFe reservoir.

3.2 Responses to variable environmental conditions

3.2.1 Sea ice melt

Spring sea ice melt provides dFe to surface waters as light becomes progressively available to primary producers. The vertical distribution of this dFe is dependent on stratification and/or mixed layer depth. The effect of dFe from sea ice melt was tested by providing this dFe source between the surface and 1, 10 and 30 m, with a maximum concentration of 0.2 nM (Table 1, equation 29).

Distribution of dFe from sea ice melt over 10 and 30 m produces similar patterns of total integrated POC, with only small differences in the magnitude of the *P. antarctica* and diatom blooms (Fig. 5A). Confinement of the sea ice-derived dFe to surface waters (1 m) allows *P. antarctica* colonies to dominate the bloom (Figure 5B). Diatoms become the dominate taxa when the sea ice dFe is distributed over depths more than 10 m (Figure 5C). Independent of the depth over which the sea ice-derived dFe is distributed, the bloom starts in early November and *P. antarctica* reaches maximum biomass in mid-December (Fig. 5B). The maximum total primary productivity of *P. antarctica* colonies shifts from early January to mid-December when the sea ice-derived dFe is available

shallower than 10 m, which lowers the available dFe supply. Distribution deeper than 10 m provides more sea ice-derived dFe and diatoms become dominant (Fig. 5C).

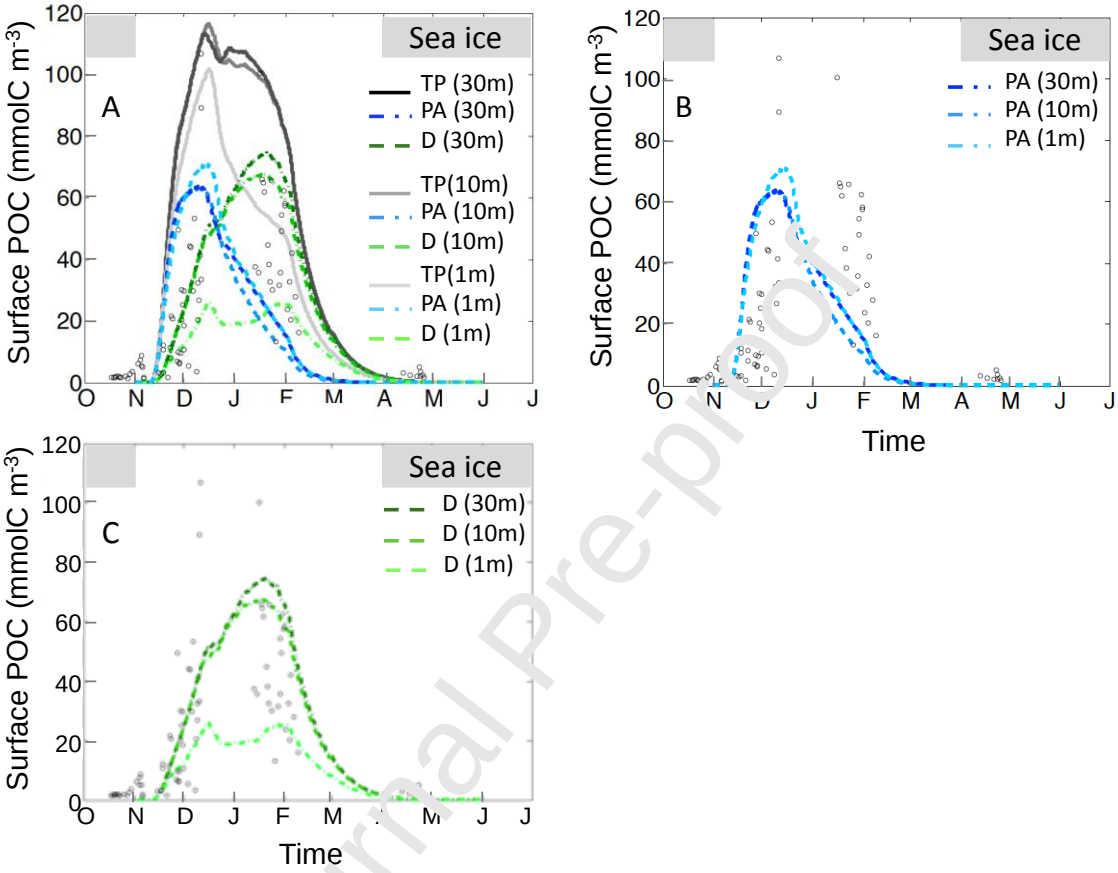

Figure 5: Simulated time evolution of surface A) particulate organic carbon (POC), B) *P. antarctica* POC and C) diatom POC obtained for input of sea ice-derived dFe that is distributed over 30 (black line), 10 (dark grey line) and 1 m (light grey line). Surface POC is calculated using total phytoplankton (TP, solid line), *P. antarctica* (PA: solitary cells and colonies, blue dash-dot line), and diatoms (D, green dashed lines). Observed values (circles) are from field measurements made in the Ross Sea (Smith et al., 2000).

3.2.2 Mid-Water Inputs

Mixing of iron-rich mid-water with surface water at 5 and 90-day intervals (Table 1), which bracket the observed frequency of mesoscale eddies and MCDW intrusions in the Ross Sea (Mack et al., 2017), provide an evaluation of the effect of mid-water dFe inputs on phytoplankton bloom characteristics. Input of mid-water dFe every 5 days maintains water column concentrations that are higher than those produced by recharge of dFe every 90 days.

For both simulations, the phytoplankton bloom starts at the beginning of November and persists until April (Fig. 6A, B). The simulated surface POC shows a maximum in December, which is followed by a second smaller maximum that extends throughout the growing season (Fig. 6A, B). Unlike in the base case, diatoms dominate the first POC maximum and the bloom of *P. antarctica* is shifted into the latter part of the growing season (Fig. 6C, D).

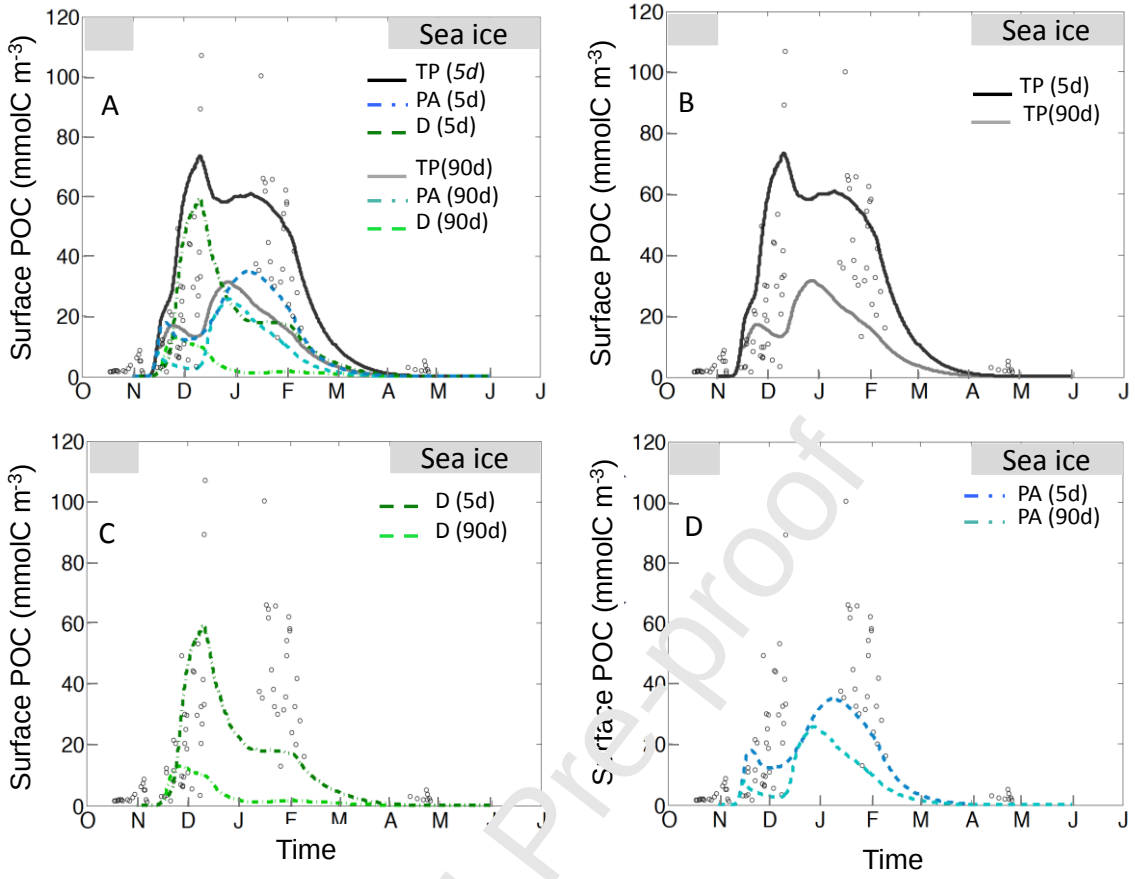

Figure 6: Simulated time evolution of surface A) particulate organic carbon (POC), B) total phytoplankton POC, C) diatom POC, and D) *P. antarctica* POC obtained with mid-water inputs of dFe at 5-day (black line) and 90-day intervals (grey line) and distributed between the surface and 100 m. Surface POC is obtained for total phytoplankton (TP, solid line), *P. antarctica* (PA: solitary cells and colonies, blue dash-dot lines), and diatoms (D, green dashed lines). Observed values (circles) are from field measurements made in the Ross Sea (Smith et al., 2000).

The POC production generated with a 5-day input of dFe is about 66% of that produced in the base case and that produced by MW dFe recharge is 30% of the base case (cf. Fig. 3C). The higher dFe concentrations from the 5-day inputs support a large bloom

in early December, which quickly decreases in early January (Fig. 6C). The lower water column dFe concentration (90-day input) favors a small initial diatom bloom (10 mmol C m^{-3}) in mid-November followed by a large *P. antarctica* bloom that is maximal in mid-December and decreases slowly until March (Fig. 6C, D). The higher water column dFe concentration supports development of a small *P. antarctica* bloom in mid-November, which is followed by a larger haptophyte bloom that begins in January and reaches a maximum value of 38 mmol C m^{-3} (Fig. 6C, D). The high dFe concentrations allow *P. antarctica* and diatoms to reach their respective maximum values 10 to 15 days later than the low dFe concentration.

In both simulations, dFe concentrations are reduced to less than 0.05 nM, suggesting that phytoplankton consume all the iron supplied by MW inputs. Over the growing season, phytoplankton remove about 4.8 nmol when dFe is supplied at 5-day intervals and 0.27 nmol when dFe is supplied over 90-day intervals.

3.2.3 Sediment iron inputs

The effect of dFe provided by suspension of continental shelf bottom sediments and shallow banks was considered with simulations in which the only source of dFe was at 550 and 300 m, respectively (Table 1, Sed-1 to Sed-4). For these simulations, a constant dFe concentration of 0.6 nM was specified between 550m and 300m and the seafloor. For both scenarios, the simulated total surface POC was about 18% of observed values (Fig. 7A, B). The total POC is composed of a large diatom bloom that occurred between November and January and a double bloom of *P. antarctica* that consists of a small short duration bloom in early November and a larger longer duration bloom that

reaches a maximum in early January. The early season diatom bloom and later *P. antarctica* bloom differ from the base case simulation and from the phytoplankton growth sequence observed in the Ross Sea.

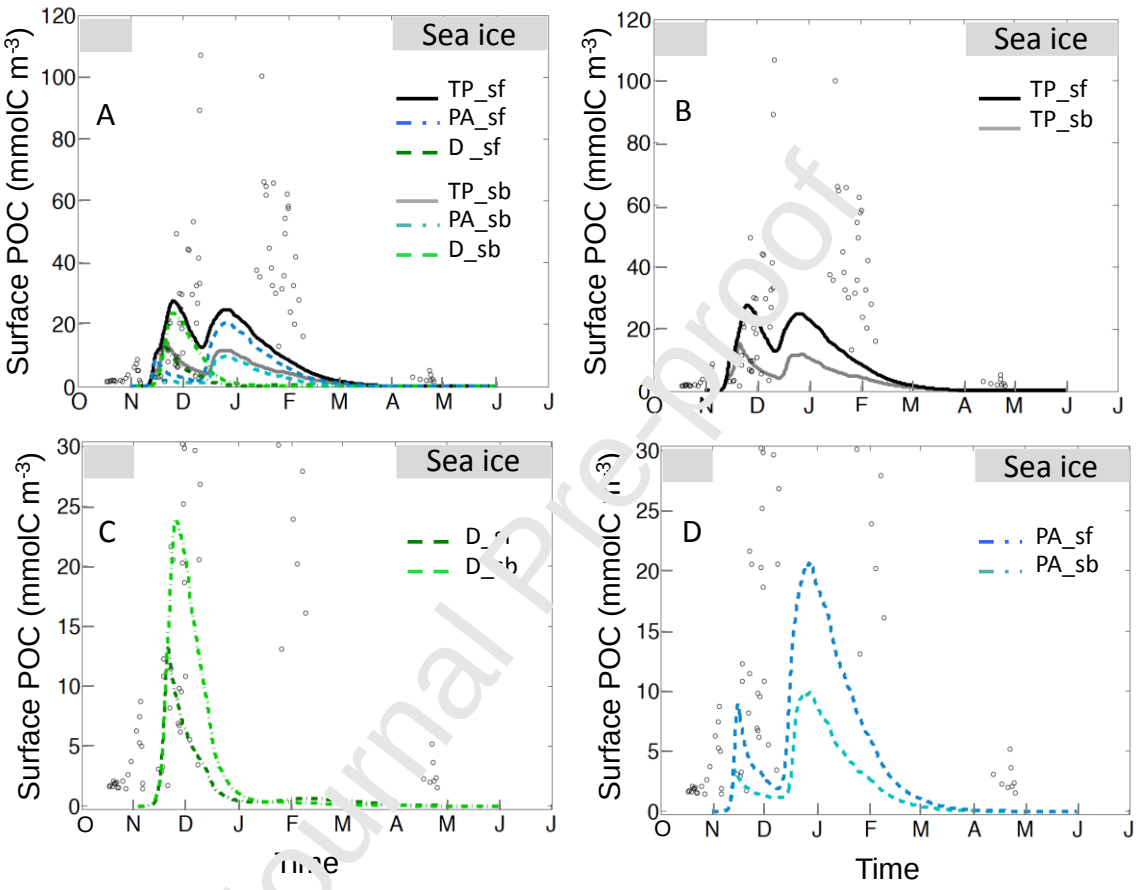

Figure 7: Simulated time evolution of surface A) particulate organic carbon (POC), B) total phytoplankton POC, C) diatom POC, and D) *P. antarctica* POC obtained with inputs of dissolved iron from sediments resuspended from the seafloor at 550 m (sf, grey lines) and a shallow bank at 300 m (sb, black lines). Surface POC is obtained for total phytoplankton (TP, solid lines), *P. antarctica* (PA: solitary cells and colonies, dash-dot lines), and diatoms (D, dashed lines). Observed values (circles) are from field measurements made in the Ross Sea (Smith et al., 2000).

3.2.4 Sea ice cover and surface mixing

Bloom dynamics respond to variability in sea ice cover, which modifies the light and mixing regimes. The effect of variable sea ice cover was tested with simulations that included lengthening the time of open water (no sea ice cover) and dFe provided by MW sources and bottom sediments (Table 1).

Removal of sea ice reduces the magnitude of the bloom produced by dFe supplied from mid- and deep water relative to the bloom that occurs when sea ice is present (Fig. 8A, B). The presence of sea ice enhances total POC production, but the bloom is delayed by about one week and ends sooner relative to the no sea ice scenario. The response of diatoms to the absence of sea ice is essentially the same as that for the presence of sea ice, except for a delay in the occurrence of the maximum production by a few days when sea ice is not present (Fig. 8C). The magnitude of the *P. antarctica* bloom almost doubles when sea ice is present (Fig. 8D).

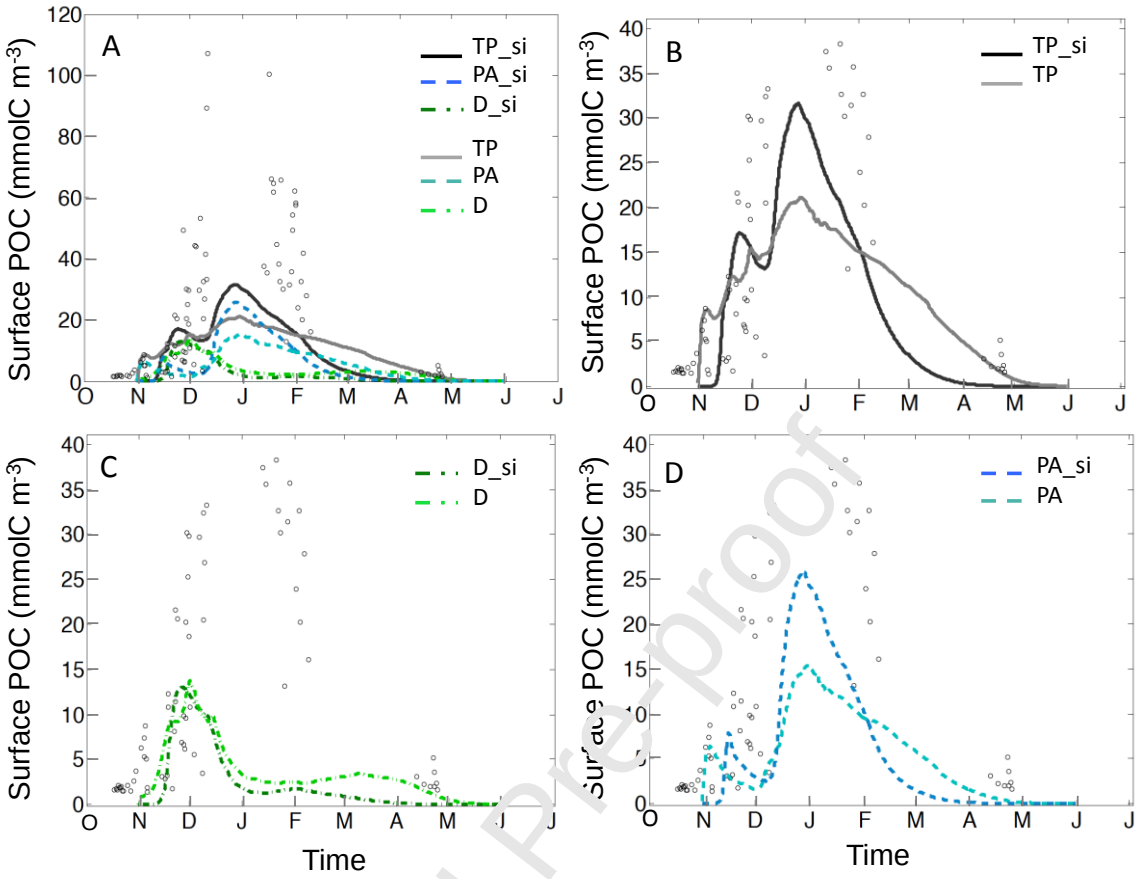

Figure 8: Simulated time evolution of surface A) particulate organic carbon (POC), B) total phytoplankton POC, C) diatom POC, and D) *P. antarctica* POC obtained with inputs of dissolved iron from MW sources at 90-day intervals distributed between the surface and 100 m with (si, black lines) and without (grey lines) sea ice cover. Surface POC is obtained for total phytoplankton (TP, solid lines), *P. antarctica* (PA: solitary cells and colonies, dash-dot lines), and diatoms (D, dashed lines). Observed values (circles) are from field measurements made in the Ross Sea (Smith et al., 2000).

The absence of sea ice enhances vertical mixing which recharges the water column dFe from bottom sediment and shallow bank sources. These inputs support a low level of phytoplankton production that extends from November to late April (Fig. 9A, D).

In contrast, the presence of sea ice supports higher initial surface POC production that then declines to zero by March. For both scenarios, diatoms dominate the initial bloom from early November to December (Fig. 9C, F). *P. antarctica* begins to bloom in late December and then dominates the phytoplankton assemblage for the remainder of the growing season (Fig. 9B, E).

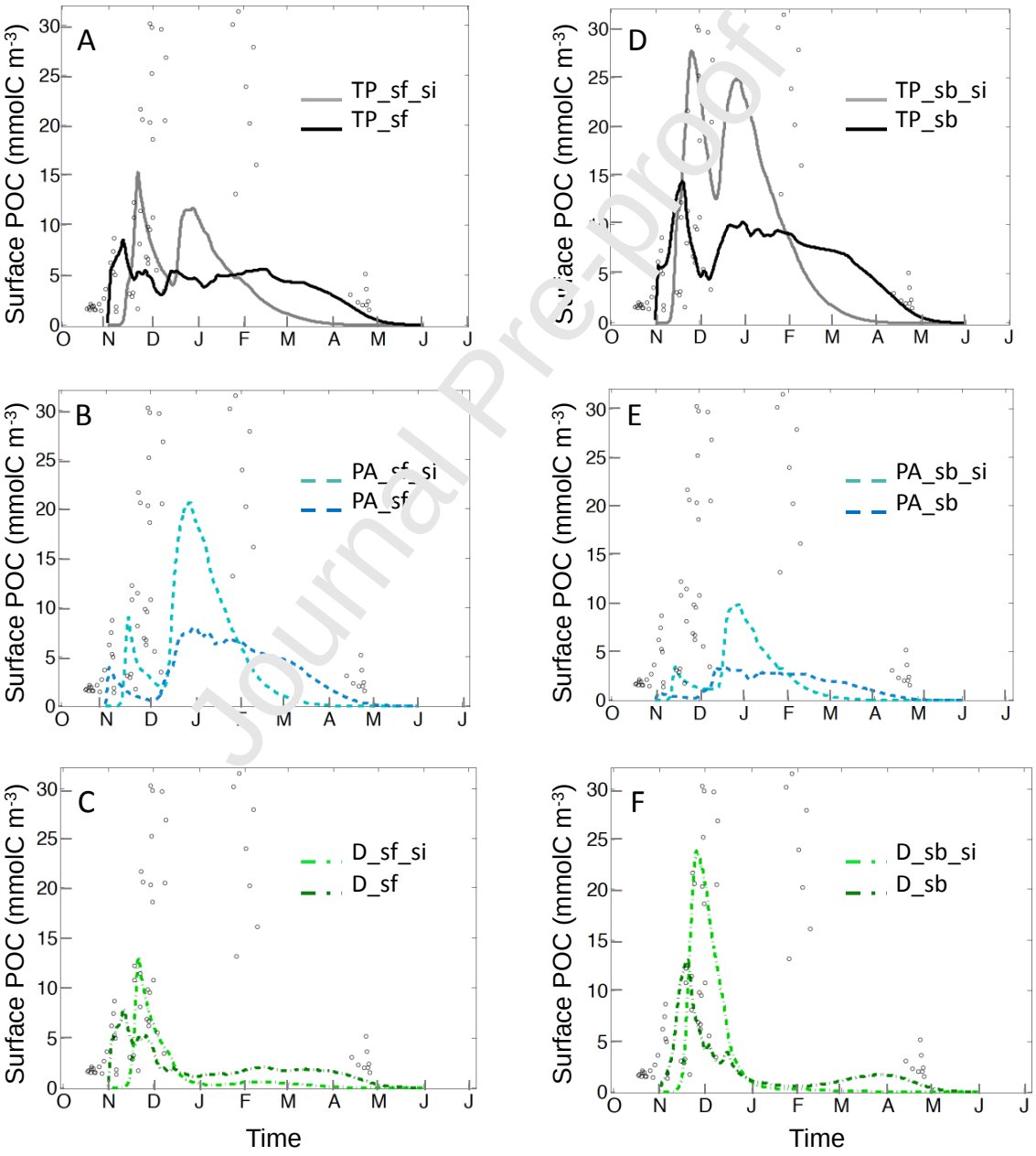

Figure 9: Simulated time evolution of surface particulate organic carbon (POC) for total phytoplankton (A, D), *P. antarctica* POC (B, E) and diatom POC (C, F) obtained with dissolved iron (dFe) inputs from the seafloor (sf) and shallow bank (sb) with (si, grey lines) and without (black lines) sea ice cover. The shadow bank inputs (sb, dashed lines) provide dFe between 300 m and the bottom and sea floor inputs (sf, solid lines) provide dFe between 550 m and the bottom. Surface POC is obtained for total phytoplankton (TP), *P. antarctica* (PA: solitary cells and colonies), and diatoms (D). Observed values (circles) are from field measurements made in the Ross Sea (Smith et al., 2000).

3.2.5 Budget analysis

Mean daily phytoplankton production, Fe:C ratios, and dFe recycling and demand were estimated from the cumulative seasonal budget obtained for each simulation (Table 2, supplementary document C). For all dFe sources, diatom net production was higher than *P. antarctica* net production. Diatom daily net production is one order of magnitude greater than *P. antarctica* daily net production and accounts for most of the total phytoplankton production (Table 2). The mean daily net production of *P. antarctica* colonies is one to three orders of magnitude lower than that obtained for *P. antarctica* solitary cells (Table 2). Parameter values for the two stages are similar (Table S2), suggesting that the difference between *P. antarctica* flagellate and colonial production reflects the benefit of a two-stage growth strategy.

Table 2: Mean daily net primary production (mmol C m^{-2} d^{-1}) of diatoms, *P. antarctica* solitary cells and colonies, and total phytoplankton obtained from simulations with and without sea ice cover and different sources of dissolved iron.

	Simulation	Reference	Net production (mmol C m^{-2} d^{-1})			
			Diatoms	*P. antartica* solitary cells	*P. antartica* colonies	Total phytoplankton
Sea ice cover	Base case	BC	230	29	0.04	259
	Sea ice supply	SI-1	253	32	0.04	285
	Sea ice supply	SI-2	315	31	0.90	347
	Sea ice supply	SI-3	297	35	0.04	332
	MW supply	MW-1	130	16	0.41	147
	MW supply	MW-2	250	23	1.30	274
	Sediment supply	Sed-1	52	8	0.17	60
	Sediment supply	Sed-2	100	12	0.21	112
Sea ice free	MW supply	MW-3	134	19	0.58	154
	Sediment supply	Sed-3	45	8	0.14	52
	Sediment supply	Sed-4	88	14	0.41	102

The dFe demand was calculated using the approach given in Kutska et al. (2015) (Method 1, Table 3) and estimated from the average dFe uptake obtained for each simulation (Method 2, Table 3). The approach used by Kutska et al. (2015) is based on net production and an average Fe:C ratio, which were calculated for each simulation and are given in Table 2 and Table 4, respectively. Also, the contribution of dFe recycled via remineralization of phytoplankton loss from mortality, zooplankton grazing and detrital decomposition relative to the total dFe uptake was calculated from each simulation (Table 3).

Table 3: Iron demand of diatoms, *P. antarctica* solitary cells and colonies, and total phytoplankton calculated from simulations with and without sea ice cover and different sources of dissolved iron (dFe). Method 1 is based on Kustka et al. (2015) and uses net production (Table 2) multiplied by the average Fe:C ratio (Table 4). Method 2 is based on the daily seasonal dFe uptake obtained for each simulation (supplementary document B). Recycled dFe is the fraction of loss from phytoplankton mortality, zooplankton grazing and detrital decomposition that is remineralized relative to the total uptake of dFe by diatoms, *P. antarctica* solitary cells and colonies.

	Simulation	Reference	dFe demand (Method 1) (nmol m^{-2} d^{-1})				dFe demand (Method 2) (nmol m^{-2} d^{-1})				dFe recycled (%)
			Diatoms	*P. antartica* solitary cells	*P. antartica* colonies	Total phytoplankton	Diatoms ($x10^{-3}$)	*P. antartica* solitary cells	*P. antartica* colonies ($x10^{-5}$)	Total phytoplankton	Total phytoplankton
Sea ice cover	Base case	BC	2691	362	0.45	3053	42.83	8246	3.47	8250	2.26
	Sea ice supply	SI-1	2809	396	0.47	3205	0.26	7344	1.53	7340	2.75
	Sea ice supply	SI-2	3051	349	9.31	3409	0.28	2664	2.04	2660	7.91
	Sea ice supply	SI-3	3889	480	0.45	4369	0.30	6970	2.28	6970	3.61
	MW supply	MW-1	371	58	1.32	430	0.12	514	0.08	514	5.72
	MW supply	MW-2	1466	214	10.70	1690	0.22	3067	0.10	3070	4.41
	Sediment supply	Sed-1	80	19	0.39	99	0.08	442	0.04	442	1.57
	Sediment supply	Sed-2	67	34	0.55	102	0.17	557	0.11	557	3.10
Sea ice free	MW supply	MW-3	528	111	2.91	641	0.12	1325	0.18	1320	3.35
	Sediment supply	Sed-3	90	26	0.42	117	0.03	842	0.02	842	0.87
	Sediment supply	Sed-4	273	78	2.05	354	0.08	922	0.07	922	3.03

Table 4: Average Fe:C ratios (μmol Fe:mol C) of diatoms, *P.antarctica* solitary cells and colonies, and total phytoplankton calculated from simulations with and without sea ice cover and different sources of dFe. The Fe:C ratio for each phytoplankton component is calculated using the phytoplankton associated dFe and phytoplankton biomass.

	Simulation	Reference	Average Fe:C ($\mu mol\ mol^{-1}$)			
			Diatoms	*P. antartica* solitary cells	*P. antartica* colonies	Total phytoplankton
Sea ice cover	Base case	BC	11.7	12.3	11.2	11.6
	Sea ice supply	SI-1	11.1	12.4	11.3	11.2
	Sea ice supply	SI-2	9.7	11.2	10.3	10.1
	Sea ice supply	SI-3	13.1	13.9	12.2	12.9
	MW supply	MW-1	2.8	3.6	3.2	3.2
	MW supply	MW-2	5.9	9.4	8.3	7.1
	Sediment supply	Sed-1	1.5	2.5	2.2	2.0
	Sediment supply	Sed-2	0.7	2.8	2.5	2.0
Sea ice free	MW supply	MW-3	3.9	5.7	5.0	4.7
	Sediment supply	Sed-3	2.0	3.5	3.0	2.4
	Sediment supply	Sed-4	3.1	5.6	5.0	4.4

The average Fe:C ratios calculated from the simulations range from 2.0 to 12.9 μmol mol^{-1}. These ratios are consistent with estimates provided by Twinning et al. (2004) and Strzepek et al. (2011), which range from 6 to 14 μmol mol^{-1} and 0.4 to 8.6 μmol mol^{-1}, respectively. For all simulations, the Fe:C ratio of *P. antarctica* solitary cells is higher than that for diatoms, as observed by Strzepek et al. (2011) for Southern Ocean isolates.

Kutska et al. (2015) estimated average Fe:C ratios of 1.51 to 2.06 μmol mol^{-1} at locations around shallow banks in the Ross Sea (e.g. Pennell Bank). The Fe:C ratios estimated from the simulations that consider dFe inputs from shallow sediment sources (Sed-1, Sed-2, Table 4) agree with these field-based values. Simulations with dFe inputs

from sea ice result in Fe:C ratios that are higher than those obtained with MW and sediment dFe sources (Table 4). The absence of sea ice results in average Fe:C ratios that are lower relative to simulations with sea ice present (MW-3 vs. MW-1, Sed-3,4 vs. Sed-1,2, Table 4). This suggests that dFe uptake is higher with sea ice present because the net production is similar between simulations with and without sea ice (Table 2).

The dFe demand estimated with Method 1 is less than that obtained with Method 2 except for simulation SI-2, 3,410 nmol Fe m^{-2} d^{-1} versus 2,660 nmol Fe m^{-2} d^{-1} (Table 3). Also, Method 1 shows the largest dFe demand from diatoms whereas Method 2 shows the highest demand from *P. antarctica* solitary cells. This difference is from the approach used with Method 1 using mean daily net production (higher for diatoms) and Method 2 using seasonal mean daily dFe uptake.

The percent recycled dFe and dFe demand, estimated from Method 2, do not show an obvious relationship (Table 3). The maximum percentage of recycled dFe (7.91%) is associated with the presence of sea ice (SI-2, Table 3) and the highest dFe demand is attained in the base case and sea ice simulations (BC, SI-1, Table 3). The lowest percentage of recycled dFe is obtained when sediments are the primary dFe source (Sed-3, Table 3) and the lowest dFe demand (using Method 2) is obtained from the simulation that included mid-water dFe inputs (MW-1, Table 3).

4. Discussion

4.1 Productivity, iron demand and recycling

The highest rates of simulated net production, 285 and 347 mmol C m^{-2} d^{-1}, were obtained from simulations that included dFe inputs from melting sea ice cover. Inputs of

dFe from MW sources sustain a simulated primary production of 147-274 mmol C m^{-2} d^{-1}. Sediment sources of dFe supported production rates of 52-112 mmol C m^{-2} d^{-1}. Arrigo et al. (2008) estimated mean daily primary productivity rates between 1997-2006 in the Ross Sea that ranged from 13 to 237 mmol C m^{-2} d^{-1}. Smith and Kaufman (2017) estimated rates of 28 to 190 mmol C m^{-2} d^{-1} for the Ross Sea polynya and 33 to 180 mmol C m^{-2} d^{-1} for the western Ross Sea. These estimates are slightly lower than the primary production rates obtained from the simulations. However, the field-based estimates represent average production over large regions and the simulated estimates are based on a small region. For comparison, primary productivity rates of 97 - 518 mmol C m^{-2} d^{-1} were measured in December 1994 in the Ross Sea polynya (Smith and Gordon, 1997).

Of the idealized simulations used in this study only the base case included inputs of dFe from sea ice, mid-water and sediment sources. The scenario simulations considered contributions of different dFe sources. The simulation that considered dFe inputs from deep sediments (Sed-1, 622 m) showed a sustained rate of primary production of 60 mmol C m^{-2} d^{-1}. Gerringa et al. (2015) estimated that 75 mmol C m^{-2} d^{-1} in the Ross Sea polynya in early summer was maintained by vertical diffusion of dFe from seafloor sediments to the upper water layers.

Kutska et al. (2015) estimated that the early summer net production after sea ice melt around shallow banks in the Ross Sea of 56 to 105 mmol C m^{-2} d^{-1} is supported by dFe supplied by vertical inputs from 100-200 m. The simulated primary production rates obtained with only dFe supplied from bottom sediments are consistent with these estimates. However, Kutska et al. (2015) identified a hot spot of productivity, 300-457

mmol C m^{-2} d^{-1}, associated with depths shallower than 300 m and suggested that the additional production was supported by dFe provided by MCDW. The simulated primary production rates obtained with dFe inputs from shallow sediments (102-112 mmol C m^{-2} d^{-1}) or from MW inputs (274 mmol C m^{-2} d^{-1}), while lower than observed rates, are the highest simulated values. The simulated production supported by sediment dFe inputs are likely underestimates because the model does not include mixing associated with flow over a shallow bank; rather dFe is simply increased from the seafloor to 300 m. This simulation configuration represents diffusion of dFe and vertical mixing of the upper water layers, but not the circulation processes associated with a shallow bank. The only simulated phytoplankton productivity (347 mmol C m^{-2} d^{-1}) that was of the same magnitude as observed for the hot spot included dFe inputs to surface waters from melting sea ice in the early growing season. This suggests that the magnitude of the summer bloom may be connected to earlier phytoplankton production. Thus, the magnitude of the total phytoplankton bloom is determined by the relative contributions of different iron sources and dFe provided by melting sea ice is essential for maintaining the high primary productivity rates that are observed in early spring.

The dFe demand estimated from the simulated Fe:C ratios and the net production values, the approach used by Kutska et al. (2015), for dFe sediment inputs ranged from 99 to 102 nmol m^{-2} d^{-1}. The dFe demand estimated from field observations for shallow banks during early summer ranged from 84 to 187 nmol m^{-2} d^{-1} (Kutska et al. 2015). The simulated primary production obtained from dFe inputs from sea ice melt is more similar to that estimated for the hot spot region. However, the Fe:C ratio estimated for the hot spot region was 1.74 μmol mol^{-1} (Kutska et al. 2015), whereas the ratio estimated from

the sea ice melt simulation was 10 μmol mol^{-1}. Consequently, the simulated dFe demand obtained from the sea ice melt simulation of 3410 nmol m^{-2} d^{-1} does not match dFe demand estimated for the hot spot (Kutska et al. 2015). Rather, simulations that included dFe inputs from shallow bank sediments resulted in dFe demands of 102 to 354 nmol m^{-2} d^{-1} that matched best the field-based estimates of 521 to 794 nmol m^{-2} d^{-1}. These simulation results support the hypothesis that dFe inputs from sea ice melt in early spring trigger a phytoplankton bloom, which depletes dFe resulting in reduced dFe uptake and reduced biogenic iron cellular content. However, the phytoplankton assemblage maintains subsequent productivity by dFe supplied from mid- and deep-water sources.

Using a mean satellite-derived surface chlorophyll a concentration of 1.95 μg Chl a L^{-1} and Fe:C ratios of 0.4 to 8.6 μmol mol^{-1}, Gerringa et al. (2015) estimated the dFe requirement needed to sustain the Ross Sea polynya phytoplankton bloom to be 40 - 910 nmol Fe m^{-2} d^{-1}. Similar simulated surface chlorophyll values were obtained from simulations that included dFe inputs from mid-water sources (MV1) and bottom sediments (Sed-1, Sed-2). The dFe demand estimated from these simulations (using Method 2) was 514, 442 and 557 nmol Fe m^{-2} d^{-1}, respectively. Simulations without sea ice cover and dFe inputs from sediments (Sed-3, Sed-4) had higher dFe demands of 842 and 922 nmol Fe m^{-2} d^{-1}, which correspond to the upper range estimated by Gerringa et al. (2015). However, the simulated Fe:C ratios of 2.4 and 4.4 μmol mol^{-1} are lower than the upper ratio value of 8.6 μmol mol^{-1} used by Gerringa et al. (2015) and simulated surface chlorophyll concentrations were less than 1 μg Chl L^{-1}. These simulation results suggest that the dFe demand is sensitive to the adaptive strategy of diatoms and *P. antarctica* to light and nutrient availability during the growing season.

Kutska et al. (2015) proposed that phytoplankton production in the Ross Sea can be sustained by recycled dFe. The simulations support this suggestion, but show a complex interaction between recycling and external sources of dFe. The biogeochemical model dynamics allow a fraction of dFe in the phytoplankton, zooplankton fecal pellets, and detrital pool to be recycled and become available for phytoplankton uptake. The percentage of the recycled dFe used by phytoplankton depends on the strength of external dFe sources. The fraction of biogenic dFe that is recycled is highest (3 to 7%) for simulations with significant external dFe sources, such as sea ice melt and mid-water inputs, and reliance on uptake of recycled dFe is decreased. The lack of sea ice reduces dFe recycling. Inputs of dFe from deep sediments have lower recycling of dFe (less than 1%) and more dependence on this pool to sustain simulated production. The implication is that the recycled dFe pool can be important for sustaining production in some regions and at specific times within the growing season.

4.2. The role of sea ice

Sea ice modifies light availability, provides dFe to surface waters, and moderates the intensity of mixing of the upper water column. Sea ice captures and accumulates some iron from aerosols during the winter season or from surface water during sea ice formation (Lannuzel et al., 2016). As sea ice melts in spring, dFe is rapidly released into the surface waters coincident with increasing light availability. In the simulations, the spring retreat of sea ice produces open water allowing for increased vertical mixing, which reduces water stratification and increases transport of dFe in the water column

(Fig. 10). However, this vertical mixing is not sufficient to recharge the upper water column where phytoplankton grows.

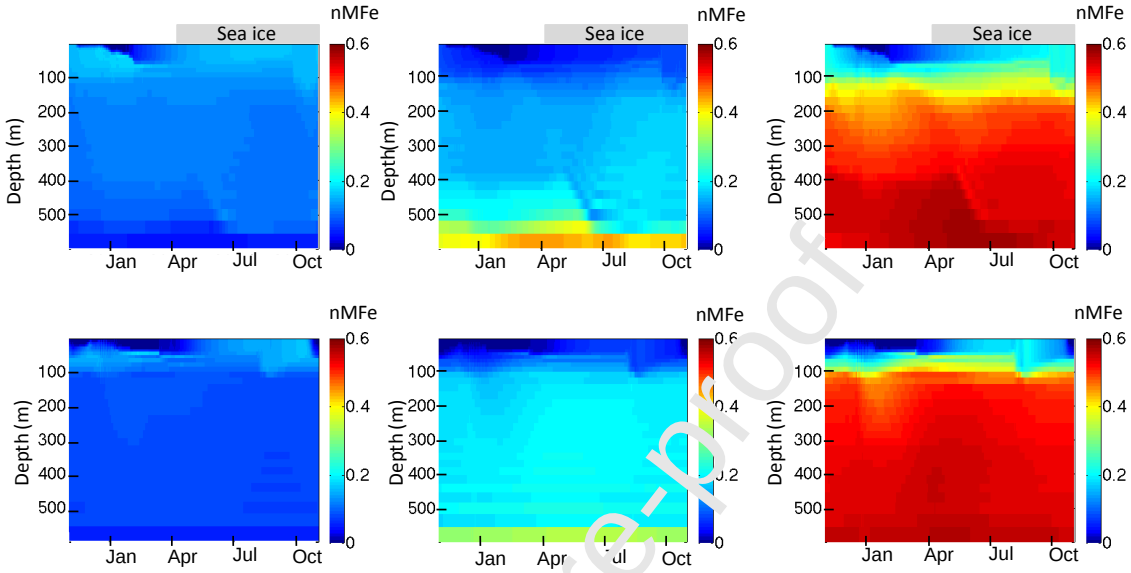

Figure 10: Simulated depth-time distribution of dissolved iron concentration with inputs from iron-rich mid-water (left column), suspension of sediment from the seafloor at 550 m (middle column) and shallow bank at 300 m (right column). The simulations were done with (upper row) and without sea ice (lower row).

The suspension of bottom sediments at 600 m or from a shallow bank represents an important source of dFe, but the time scales over which this is input to the surface waters are slow and support only a small bloom of 1 to 4 μg Chl L^{-1} (Fig. 10, middle and right panels, Figure SC25-A, SC27-A, SC29-A, SC31-A) as observed for shallow banks in the Ross Sea (Kustka et al., 2015; Smith and Kaufman, 2018). Rather, this source is important in providing the overwinter recharge of dFe to the mid- and surface waters. Sedwick et al. (2011) estimated that the efflux of dFe from depths >400 m is sufficient to provide the winter reserve dFe inventory at the start of the growing season. Field-based

observations also showed that shallow bathymetry provides dFe inputs to the euphotic zone throughout the year (Sedwick et al., 2011; Kustka et al., 2015; Gerringa et al., 2015; Hatta et al., 2017). A budget of dFe supply and demand constructed for the Ross Sea (McGillicuddy et al. 2015) showed that benthic sources contribute more than 40% of the winter reserve dFe. The simulated dFe depth-time profiles obtained with deep and shallow dFe sources (Fig. 10) are consistent with these observed and budget model results.

Removal of sea ice significantly changes the distribution and availability of dFe (Fig. 10, lower panels). Without sea ice, dFe concentrations are higher and more evenly distributed over the upper water column. However, without sea ice the water column is more stratified and has shallower mixed layers, which is supported by the distribution of the vertical momentum terms (Figs. S1, S2). McGillicuddy et al. (2015) suggested that convective mixing in winter set up the winter reserve of dFe that supported phytoplankton growth in the spring. Continued convective mixing during the growing season provides the dFe from MW inputs to the surface waters. Sea ice modifies dFe inputs to Ross Sea surface waters and its vertical distribution. The projected earlier retreat of sea ice in the Ross Sea and longer periods of open water during the growing season (Smith et al. 2014) will significantly modify the source and magnitude of dFe inputs to surface waters and its vertical distribution. The extent to which this will modify the current pattern of phytoplankton blooms is unknown.

4.3. Dissolved iron sources

The simulations show that the timing and magnitude of phytoplankton blooms and related primary production in the Ross sea are sensitive to the source of dFe and its distribution in the water column. The dFe from the winter reserve and that released early in the growing season by melting sea ice are essential for stimulating a *P. antarctica* bloom with concentrations of more than 4 μg Chl L^{-1} and subsequent regulation of the bloom magnitude (Fig. 11). The dFe provided by MW inputs is sufficient to support growth that is 25 to 50% of the magnitude of the total observed phytoplankton bloom, for recharge frequencies of 90 to 5 days, respectively. The suspension of bottom sediments contributes iron that is sufficient to support about 10% of the magnitude of the entire simulated bloom obtained in the base case. The MW inputs and the bottom iron sources selectively favor diatom growth in the spring and delay development of the *P. antarctica* bloom to the summer. Each source of dFe exerts a different control on phytoplankton bloom timing and magnitude. It is the sequencing of these inputs that results in the observed progression from an early season *P. antarctica* bloom to mid-summer diatom bloom.

McGillicuddy et al. (2015) showed that the two largest sources of dFe are from regional scale convective mixing that supplies benthic dFe to the euphotic zone in winter (about 40%) and melting sea ice (about 40%). Most of the remaining 20% of the dFe source was estimated to be supplied by MW inputs. The one-dimensional implementation of the model used in this study does not allow direct comparison with the regional budget provided in McGillicuddy et al. (2015), but the relative importance of the dFe sources is similar in both analyses.

The seasonal transfer and fate of water column dFe differs depending on the source (Fig. 11). In early spring, before bloom initiation, the surface water (surface to 100 m) contains about 19% of the total water column dFe. Mid-water column (100 to 500 m) dFe is about 57% of the total and the bottom water column (500 to 650 m) contains about 24% of the total. In the early growing season, the first bloom of *P. antarctica* rapidly depletes surface dFe and accounts for the mid-November to early December decrease. This reduction in the surface water dFe correlates in time and in magnitude with the relative increase of iron in the mid-water column, suggesting a rapid recharge from MW inputs. A second rapid depletion of surface water dFe occurred between mid-December and late January corresponding to the simulated diatom bloom (Fig. 11). Vertical transfer of iron from the mid- and bottom water column occurs, but is insufficient to maintain surface dFe concentrations relative to removal by phytoplankton uptake. This iron transfer corresponds to about 15% of the total water column dFe, half of which is in the mid-water column and the other half is in the bottom (Fig. 11).

From the end of January to early March, surface water dFe is used by the diatom bloom and eventually is completely depleted. By about mid-June recharge processes from mid- and deep-water inputs restore the relative water column dFe concentration to early spring magnitude and vertical distribution.

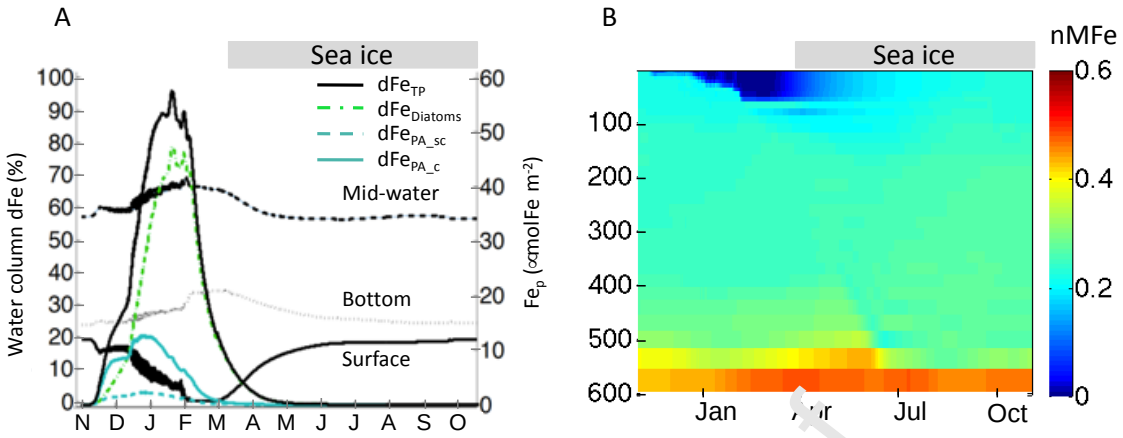

Figure 11: A) Contribution of dissolved iron (dFe) sources to total water column dFe concentration for the base case simulation as the percent of dFe in the surface waters (solid black line), middle water column (dotted black line) and bottom water column (dashed light grey line) and the percent dFe associated with total phytoplankton (dFe_{TP}, solid black line), diatoms ($dFe_{Diatoms}$, green dotted dashed line), *P.antarctica* solitary cells (dFe_{PA_sc}, blue dashed line) and colonies (dFe_{PA_c}, blue solid line). B) Time-depth distribution of dFe showing surface depletion by phytoplankton uptake and inputs from sea ice melt and sediment resuspension. The presence of sea ice is indicated (grey bar).

4.4 Conceptual model of bloom dynamics

The simulations provide insights into the complex interactions among environmental conditions and phytoplankton growth that allow a conceptual model of phytoplankton bloom dynamics in the Ross Sea to be developed (Fig. 12). The early bloom of *P. antarctica* is triggered by the beginning of light availability and the simultaneous availability of dFe from the winter reserve and melting sea ice. Initially, the surface dFe concentrations and enhanced light regime favor rapid growth of *P. antarctica*. However, as surface dFe is depleted, diatoms begin to grow in the spring and

rapidly out compete *P. antarctica* as dFe levels decrease to dominate the later stages of the bloom. Over a growing season about four times more dFe is associated with diatoms than with the *P. antarctica* biomass.

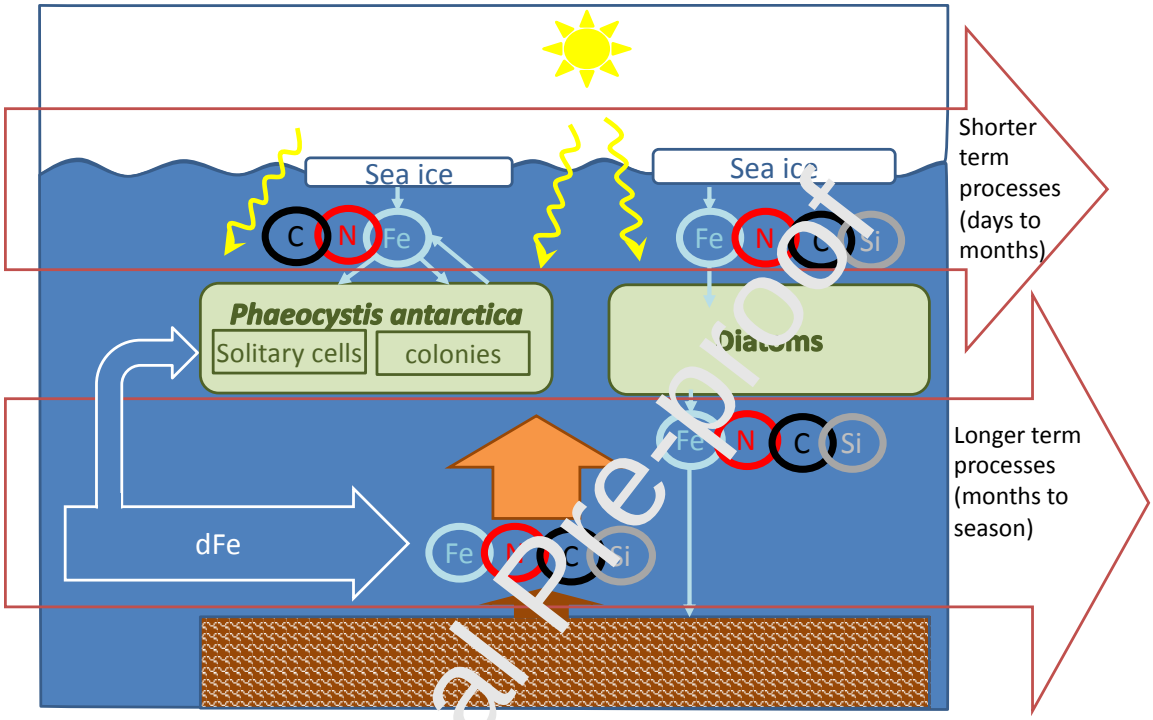

Figure 12: Conceptual model of environmental interactions that control phytoplankton blooms in the Ross sea. Surface light and nutrient inputs, especially dissolved iron (dFe) inputs from the deep-water winter reserve and melting sea ice, stimulate a *P. antarctica* bloom in early spring. Inputs of dFe via mid-water column supply sources (horizontal and vertical mesoscale eddies and MCDW inputs) and resuspension of bottom sediments maintain the bloom and allow the transition to a diatom-dominated bloom in the latter part of the growing season.

Phytoplankton bloom dynamics in the Ross Sea evolve in response to short and long time scale processes (Fig. 12). On the shorter day to month time scale, dFe

accumulates during winter in the sea ice. Sea ice melt in the spring releases this dFe, and at concentrations of 0.2 nM in the upper 10 m, is sufficient to enhance and sustain a bloom of the haptophyte, *P. antarctica*, which is simultaneously stimulated by increased light made available by sea ice retreat.

The long-term month to seasonal dFe inputs from nutrient remineralization and inputs from dFe-rich mid-water and benthic sources promote diatom growth. The largest source of recycled nitrogen in the nutrient budget is senescence of *P. antarctica* colonies, which split into solitary cells and mucus. The mucus disintegrates and contributes to the suspended particle pool before mineralization in deeper sea water. Diatom senescence provides the largest recycled contribution to the dFe reservoir. The input of nutrients from deep sources has been suggested as the mechanism that supports diatom growth along the west Antarctic Peninsula continental shelf, especially during summer (Prézelin et al. 2004). The spatial separation in the dFe inputs that support *P. antarctica* and diatom blooms in the Ross Sea suggest that each is a response to different controlling processes and that vulnerabilities to climate-induced modifications to environmental conditions will differ.

5. Conclusions

Currently, phytoplankton blooms in the Ross Sea result from short- and long-term processes that supply dFe to the surface waters. The short-term supply of dFe to surface waters via sea ice melt early in the growing season enhances the dFe provided by the winter reserve and stimulates a bloom of *P. antarctica*. Subsequent diatom blooms are supported by dFe that is provided from mid- and deep-water sources. Thus, this

combination and sequencing of dFe inputs promotes development of phytoplankton blooms in the Ross Sea that are composed about equally of haptophytes and diatoms that follow in sequence in the growing season.

The Ross Sea is projected to have reduced sea ice and longer periods of open water by 2100 (Smith et al. 2014). Reduced sea ice and earlier retreat will move the input of dFe to surface waters earlier in the growing season when light is reduced. Also, increased mixing associated with open water will change the vertical distribution of dFe and its inputs to surface waters from deeper sources. Smith et al. (2014) suggest that these conditions will favor diatom growth in the Ross Sea. However, an alternate scenario of reduced vertical mixing due to remote freshwater inputs and warmer atmospheric temperatures (Smith et al. 2014; Lannuzel et al. 2018) could reduce overall phytoplankton production in the Ross Sea. The western Antarctic Peninsula continental shelf is experiencing reductions in sea ice and longer periods of open water. The phytoplankton assemblages along this shelf are dominated by diatoms (Prézelin et al. 2000, 2004). Thus, the west Antarctic Peninsula may provide a view of future conditions for a Ross Sea with reduced sea ice.

Acknowledgments

This study is a contribution to the Processes Regulating Iron Supply at the Mesoscale-Ross Sea (PRISM) project, which was supported by NSF Antarctic Sciences grant numbers ANT-0944174 and ANT-0944254, and NSF Office of Polar Programs grant OPP-1643652. We thank an anonymous reviewer for helpful and insightful comments

that substantially improved an earlier version of the manuscript. We also thank Dr. A. Piola for editorial assistance in review of this manuscript.

References

Alderkamp, A.C., Mills, M.M., van Dijken, G.L., Laan, P., Thuróczy, C.E., Gerringa, L.J., de Baar, H.J., Payne, C.D., Visser, R.J., Buma, A.G., Arrigo, K.R., 2012. Iron from melting glaciers fuels phytoplankton blooms in the Amundsen Sea (Southern Ocean): Phytoplankton characteristics and productivity. Deep-Sea Res. II 71, 32-48. https://doi.org/10.1016/j.dsr2.2012.03.005

Arrigo, K.R., Robinson, D.H., Worthen, D.L., Dunbar, R.B., DiTullio, G.R., VanWoert, M., Lizotte, M.P., 1999. Phytoplankton community structure and the drawdown of nutrients and CO_2 in the Southern Ocean. Science 283(5400), 365-367. https://doi.org/10.1126/science.283.5400.365

Arrigo, K.R., van Dijken, G., Long, M., 2008. Coastal Southern Ocean: A strong anthropogenic CO_2 sink. Geophys. Res. Lett. 35(21). https://doi.org/10.1029/2008GL035624

Arrigo, K.R., Worthen, D.L., Robinson, D.H., 2003. A coupled ocean-ecosystem model of the Ross Sea: 2. Iron regulation of phytoplankton taxonomic variability and primary production. J. Geophys. Res. Oceans 108(C7). https://doi.org/10.1029/2001JC000856

Boyd, P.W., Watson, A.J., Law, C.S., Abraham, E.R., Trull, T., Murdoch, R., Bakker, D.C., Bowie, A.R., Buesseler, K.O., Chang, H., Charette, M., 2000. A mesoscale

phytoplankton bloom in the polar Southern Ocean stimulated by iron fertilization. Nature 407(6805), 695-702. https://doi.org/10.1038/35037500

Boyd, P.W., Lennartz, S.T., Glover, D.M., Doney, S.C., 2015. Biological ramifications of climate-change-mediated oceanic multi-stressors. Nat. Clim. Change. 5(1), 71-79. https://doi.org/10.1038/nclimate2441

Budgell, W.P., 2005. Numerical simulation of ice-ocean variability in the Barents Sea region. Ocean Dyn. 55(3-4), 370-387. https://doi.org/10.1007/s10236-005-0008-3

Cassar, N., Bender, M.L., Barnett, B.A., Fan, S., Moxim, W.J., Levy, H., Tilbrook, B., 2007. The Southern Ocean biological response to aeolian iron deposition. Science 317(5841), 1067-1070. https://doi.org/10.1126/science.1144602

Coale, K.H., Johnson, K.S., Chavez, F.P., Buesseler, K.O., Barber, R.T., Brzezinski, M.A., Cochlan, W.P., Millero, F.J., Falkowski, P.G., Bauer, J.E., Wanninkhof, R.H., 2004. Southern Ocean iron enrichment experiment: carbon cycling in high- and low-Si waters. Science 304(5669), 408-414. https://doi.org/10.1126/science.1089778

de Baar, H.J., Boyd, P.W., Coale, K.H., Landry, M.R., Tsuda, A., Assmy, P., Bakker, D.C., Bozec, Y., Barber, R.T., Brzezinski, M.A., Buesseler, K.O., 2005. Synthesis of iron fertilization experiments: from the iron age in the age of enlightenment. J. Geophys. Res. Oceans 110(C9). https://doi.org/10.1029/2004JC002601

Dinniman, M.S., Klinck, J.M., Smith Jr., W.O., 2011. A model study of Circumpolar Deep Water on the West Antarctic Peninsula and Ross Sea continental shelves. Deep-Sea Res. II 58(13-16), 1508-1523. https://doi.org/10.1016/j.dsr2.2010.11.013

Dinniman, M.S., Klinck, J.M., Bai, L.S., Bromwich, D.H., Hines, K.M., Holland, D.M., 2015. The effect of atmospheric forcing resolution on delivery of ocean heat to the Antarctic floating ice shelves. J. Clim. 28(15), 6067-6085. https://doi.org/10.1175/JCLI-D-14-00374.1

Fairall, C.W., Bradley, E.F., Hare, J.E., Grachev, A.A., Edson, J.B., 2003. Bulk parameterization of air–sea fluxes: Updates and verification for the COARE algorithm. J. Clim. 16(4), 571-591. https://doi.org/10.1175/1520-0442(2003)016<0571:BPOASF>2.0.CO;2

Feng, Y., Hare, C.E., Rose, J.M., Handy, S.M., DiTullio, G.R., Lee, P.A., Smith Jr., W.O., Peloquin, J., Tozzi, S., Sun, J., Zhang, Y., 2010. Interactive effects of iron, irradiance and CO_2 on Ross Sea phytoplankton. Deep Sea Res. Part I Oceanogr. Res. Pap., 57(3), 368-383. https://doi.org/10.1016/j.dsr.2009.10.013

Fiechter, J., Moore, A.M., Edwards, C.A., Bruland, K.W., Di Lorenzo, E., Lewis, C.V., Powell, T.M., Curchitser, E.N., Hedstrom, K., 2009. Modeling iron limitation of primary production in the coastal Gulf of Alaska. Deep-Sea Res. II 56(24), pp.2503-2519. https://doi.org/10.1016/j.dsr2.2009.02.010

Gerringa, L.J., Alderkamp, A.C., Laan, P., Thuroczy, C.E., de Baar, H.J., Mills, M.M., van Dijken, G.L., van Haren, H., Arrigo, K.R., 2012. Iron from melting glaciers fuels the phytoplankton blooms in Amundsen Sea (Southern Ocean): Iron biogeochemistry. Deep-Sea Res. II 71, 16-31. https://doi.org/10.1016/j.dsr2.2012.03.007

Gerringa, L.J.A., Laan, P., Van Dijken, G.L., van Haren, H., de Baar, H.J.W., Arrigo, K.R., Alderkamp, A.C., 2015. Sources of iron in the Ross Sea Polynya in early

summer. Mar. Chem. 177, 447-459. https://doi.org/10.1016/j.marchem.2015.06.002

Gordon, L.I., Codispoti, L.A., Jennings Jr, J.C., Millero, F.J., Morrison, J.M., Sweeney, C., 2000. Seasonal evolution of hydrographic properties in the Ross Sea, Antarctica, 1996–1997. Deep-Sea Res. II 47(15-16), 3095-3117. https://doi.org/10.1016/S0967-0645(00)00060-6

Grotti, M., Soggia, F., Ianni, C., Frache, R., 2005. Trace metals distributions in coastal sea ice of Terra Nova Bay, Ross Sea, Antarctica. Antarct. Sci. 17(2), 289-300. https://doi.org/10.1017/S0954102005002695

Haidvogel, D.B., Arango, H., Budgell, W.P., Cornuelle, B.D., Curchitser, E., Di Lorenzo, E., Fennel, K., Geyer, W.R., Hermann, A.J., Lanerolle, L., Levin, J., 2008. Ocean forecasting in terrain-following coordinates: Formulation and skill assessment of the Regional Ocean Modeling System. J. Comput. Phys. 227(7), 3595-3624. https://doi.org/10.1016/j.jcp.2007.06.016

Hatta, M., Measures, C.I., Lam, P.J., Ohnemus, D.C., Auro, M.E., Grand, M.M., Selph, K.E., 2017. The relative roles of modified circumpolar deep water and benthic sources in supplying iron to the recurrent phytoplankton blooms above Pennell and Mawson Banks, Ross Sea, Antarctica. J. Mar. Syst. 166, 61-72. https://doi.org/10.1016/j.jmarsys.2016.07.009

Ivlev, V.S., 1945. The biological productivity of waters. Uspekhi Sovrem. Biol. 19, 98-120.

Jacobs, S.S., Comiso, J.C., 1989. Sea ice and oceanic processes on the Ross Sea continental shelf. J. Geophys. Res. Oceans 94(C12), 18195-18211. https://doi.org/10.1029/JC094iC12p18195

Jacobs S.S., Giulivi C.F., 1999. Thermohaline Data and Ocean Circulation on the Ross Sea Continental Shelf. In: Spezie G., Manzella G.M.R. (eds.) Oceanography of the Ross Sea Antarctica. Springer, Milano, 3-16. https://doi.org/10.1007/978-88-470-2250-8_1

Kaufman, D.E., Friedrichs, M.A., Smith Jr., W.O., Hofmann, E.E., Dinniman, M.S., Hemmings, J.C., 2017. Climate change impacts on southern Ross Sea phytoplankton composition, productivity, and export. J. Geophys. Res. Oceans 122(3), 2339-2359. https://doi.org/10.1002/2016JC012514

Kaufman, D.E., Friedrichs, M.A., Smith Jr., W.O., Queste, B.Y., Heywood, K.J., 2014. Biogeochemical variability in the southern Ross Sea as observed by a glider deployment. Deep-Sea Res. I 92, 93-106. https://doi.org/10.1016/j.dsr.2014.06.011

Kropuenske, L.R., Mills, M.M., van Dijken, G.L., Bailey, S., Robinson, D.H., Welschmeyer, N.A., Arrigo, K.R., 2009. Photophysiology in two major Southern Ocean phytoplankton taxa: photoprotection in Phaeocystis antarctica and Fragilariopsis cylindrus. Limnol. Oceanogr. 54(4), 1176-1196. https://doi.org/10.4319/lo.2009.54.4.1176

Kustka, A.B., Kohut, J.T., White, A.E., Lam, P.J., Milligan, A.J., Dinniman, M.S., Mack, S., Hunter, E., Hiscock, M.R., Smith Jr., W.O., Measures, C.I., 2015. The roles of MCDW and deep water iron supply in sustaining a recurrent phytoplankton

bloom on central Pennell Bank (Ross Sea). Deep-Sea Res. I 105, 171-185. https://doi.org/10.1016/j.dsr.2015.08.012

Lancelot, C., Hannon, E., Becquevort, S., Veth, C., de Baar, H.J., 2000. Modeling phytoplankton blooms and carbon export production in the Southern Ocean: dominant controls by light and iron in the Atlantic sector in Austral spring 1992. Deep-Sea Res. I 47(9), 1621-1662. https://doi.org/10.1016/S0967-0637(00)00005-4

Lancelot, C., Keller, M., Rousseau, V., Smith Jr., W. O., Mathot, S., 1998. Autoecology of the Marine Haptophyte *Phaeocystis sp*. In: Anderson, D.M. et al. (Ed.) Physiological Ecology of Harmful Algal Blooms: NATO ASI Series G: Ecological sciences, Springer, 41, 209-224. http://hdl.handle.net/2013/ULB-DIPOT:oai:dipot.ulb.ac.be:2013/57906

Lannuzel, D., Schoemann, V., de Jong, J., Pasquer, B., van der Merwe, P., Masson, F., Tison, J.L., Bowie, A., 2010. Distribution of dissolved iron in Antarctic sea ice: Spatial, seasonal, and inter-annual variability. J. Geophys. Res. Biogeosci. 115, G03022. https://doi.org/10.1029/2009JG001031

Lannuzel, D., Vancoppenolle, M., van der Merwe, P., de Jong, J., Meiners, K.M., Grotti, M., Nishioka, J., Schoemann, V., 2016. Iron in sea ice: Review and new insights. Elem Sci Anth, 4, p.000130. http://doi.org/10.12952/journal.elementa.000130.

Laevastu, T., 1960. Factors affecting the temperature of the surface layer of the sea. Comment. Phys. Math. 25, 1-136.

Li, F., Ginoux, P., Ramaswamy, V., 2008. Distribution, transport, and deposition of mineral dust in the Southern Ocean and Antarctica: Contribution of major

sources. J. Geophys. Res. Atmos. 113, D10207. https://doi.org/10.1029/2007JD009190

McGillicuddy Jr., D.J., Sedwick, P.N., Dinniman, M.S., Arrigo, K.R., Bibby, T.S., Greenan, B.J.W., Hofmann, E.E., Klinck, J.M., Smith Jr., W.O., Mack, S.L., Marsay, C.M., 2015. Iron supply and demand in an Antarctic shelf ecosystem. Geophys. Res. Lett. 42(19), 8088-8097. https://doi.org/10.1002/2015GL065727

Mack, S.L., Dinniman, M.S., McGillicuddy Jr., D.J., Sedwick, P.N., Klinck, J.M., 2017. Dissolved iron transport pathways in the Ross Sea: Influence of tides and horizontal resolution in a regional ocean model. J. Mar. Syst. 166, 73-86. https://doi.org/10.1016/j.jmarsys.2016.10.008

Marsay, C.M., Sedwick, P.N., Dinniman, M.S., Barrett, P.M., Mack, S.L., McGillicuddy Jr., D.J., 2014. Estimating the benthic efflux of dissolved iron on the Ross Sea continental shelf. Geophys. Res. Lett. 41(21), 7576-7583. https://doi.org/10.1002/2014GL061684

Marsay, C.M., Barrett, P.M., McGillicuddy Jr., D.J., Sedwick, P.N., 2017. Distributions, sources, and transformations of dissolved and particulate iron on the Ross Sea continental shelf during summer. J. Geophys. Res. Oceans 122(8), 6371-6393. https://doi.org/10.1002/2017JC013068

Martin, J.H., Gordon, R.M., Fitzwater, S.E. 1990. Iron in Antarctic waters. Nature 345 (6271), 156–158. https://doi.org/10.1038/345156a0

Olson, R.J., Sosik, H.M., Chekalyuk, A.M., Shalapyonok, A., 2000. Effects of iron enrichment on phytoplankton in the Southern Ocean during late summer: active

fluorescence and flow cytometric analyses. Deep-Sea Res. II 47(15-16), 3181-3200. https://doi.org/10.1016/S0967-0645(00)00064-3

Peloquin, J.A., Smith Jr., W.O., 2007. Phytoplankton blooms in the Ross Sea, Antarctica: interannual variability in magnitude, temporal patterns, and composition. J. Geophys. Res. Oceans 112, C08013. https://doi.org/10.1029/2006JC003816

Piñones, A., Hofmann, E.E., Costa, D.P., Goetz, K., Burns, J.M., Roquet, F., Dinniman, M.S., Klinck, J.M., 2019. Hydrographic variability along the inner and mid-shelf region of the western Ross Sea obtained using instrumented seals. Prog. Oceanogr. 174, 131-142. https://doi.org/10.1016/j.pocean.2019.01.003

Platt, T., Gallegos, C.L., Harrison, W.G.,1980. Photoinhibition of photosynthesis in natural assemblages of marine phytoplankton. J. Mar. Res. 38, 687-701

Prézelin, B.B., Hofmann, E.E., Mengelt, C., Klinck, J.M., 2000. The linkage between Upper Circumpolar Deep Water (UCDW) and phytoplankton assemblages on the west Antarctic Peninsula continental shelf. J. Mar. Res. 58(2), 165-202. https://doi.org/10.1357/002224000321511133

Prézelin, B.B., Hofmann, E.E., Moline, M., Klinck, J.M., 2004. Physical forcing of phytoplankton community structure and primary production in continental shelf waters of the Western Antarctic Peninsula. J. Mar. Res. 62(3), 419-460. https://doi.org/10.1357/0022240041446173

Powell, T.M., Lewis, C.V., Curchitser, E.N., Haidvogel, D.B., Hermann, A.J., Dobbins, E.L., 2006. Results from a three-dimensional, nested biological-physical model of the California Current System and comparisons with statistics from satellite

imagery. J. Geophys. Res. Oceans 111(C7). https://doi.org/10.1029/2004JC002506

Riegman, R., Noordeloos, A.A.M., Cadée, G.C., 1992. *Phaeocystis* blooms and eutrophication of the continental coastal zones of the North Sea. Mar. Biol. 112 (3), 479–484. https://doi.org/10.1007/BF00356293

Riegman, R., van Boekel, W., 1996. The ecophysiology of *Phaeocystis globosa*: a review. J. Sea Res. 35(4), 235-242. https://doi.org/10.1016/S1385-1101(96)90750-9

Sedwick, P.N., DiTullio, G.R., Mackey, D.J., 2000. Iron and manganese in the Ross Sea, Antarctica: seasonal iron limitation in Antarctic shelf waters. J. Geophys. Res. Oceans 105(C5), 11,321-11,336. https://doi.org/10.1029/2000JC000256

Sedwick, P.N., Marsay, C.M., Sohst, B.M., Aguilar-Islas, A.M., Lohan, M.C., Long, M.C., Arrigo, K.R., Dunbar, R.B., Saito, M.A., Smith Jr., W.O., DiTullio, G.R., 2011. Early season depletion of dissolved iron in the Ross Sea polynya: Implications for iron dynamics on the Antarctic continental shelf. J. Geophys. Res. Oceans 116(C12). https://doi.org/10.1029/2010JC006553

Sherrell, R.M., Lagerström, M.E., Forsch, K.O., Stammerjohn, S.E., Yager, P.L., 2015. Dynamics of dissolved iron and other bioactive trace metals (Mn, Ni, Cu, Zn) in the Amundsen Sea Polynya, Antarctica. Elem. Sci. Anth. 3, 000071. http://doi.org/10.12952/journal.elementa.000071

Shields, A.R., Smith Jr., W.O., 2009. Size-fractionated photosynthesis/irradiance relationships during *Phaeocystis antarctica*-dominated blooms in the Ross Sea, Antarctica. J. Plankton Res. 31(7), 701-712. https://doi.org/10.1093/plankt/fbp022

Smith Jr., W.O., Ainley, D.G., Arrigo, K.R., Dinniman, M.S., 2014. The oceanography and ecology of the Ross Sea. Ann. Rev. Mar. Sci. 6, 469-487.https://doi.org/10.1146/annurev-marine-010213-135114

Smith Jr., W.O., Asper, V., Tozzi, S., Liu, X., Stammerjohn, S.E., 2011. Surface layer variability in the Ross Sea, Antarctica as assessed by in situ fluorescence measurements. Prog. Oceanogr. 88(1-4), 28-45. https://doi.org/10.1016/j.pocean.2010.08.002

Smith Jr, W.O., Dennett, M.R., Mathot, S., Caron, D.A., 2003. The temporal dynamics of the flagellated and colonial stages of *Phaeocystis antarctica* in the Ross Sea. Deep-Sea Res. II 50(3-4), 605-617. https://doi.org/10.1016/S0967-0645(02)00586-6

Smith Jr, W.O., Gordon, L.I., 1997. Hyperproductivity of the Ross Sea (Antarctica) polynya during austral spring. Geophys. Res. Lett. 24(3), 233-236. https://doi.org/10.1029/96GL03926

Smith Jr., W.O., Jones, R.M., 2015. Vertical mixing, critical depths, and phytoplankton growth in the Ross Sea. ICES J. Mar. Sci. 72(6), 1952-1960. https://doi.org/10.1093/icesjms/fsu234

Smith Jr., W.O., Kaufman, D.E., 2018. Climatological temporal and spatial distributions of nutrients and particulate matter in the Ross Sea. Prog. Oceanogr. 168, 182-195. https://doi.org/10.1016/j.pocean.2018.10.003

Smith Jr., W.O., Marra, J., Hiscock, M.R., Barber, R.T., 2000. The seasonal cycle of phytoplankton biomass and primary productivity in the Ross Sea, Antarctica.

Deep-Sea Res. II 47(15-16), pp.3119-3140. https://doi.org/10.1016/S0967-0645(00)00061-8

Smith Jr., W.O., Tozzi, S., Long, M.C., Sedwick, P.N., Peloquin, J.A., Dunbar, R.B., Hutchins, D.A., Kolber, Z., DiTullio, G.R., 2013. Spatial and temporal variations in variable fluoresence in the Ross Sea (Antarctica): Oceanographic correlates and bloom dynamics. Deep-Sea Res. I 79, 141-155. https://doi.org/10.1016/j.dsr.2013.05.002

Strzepek, R.F., Maldonado, M.T., Hunter, K.A., Frew, R.D., Boyd, P.W., 2011. Adaptive strategies by Southern Ocean phytoplankton to lessen iron limitation: Uptake of organically complexed iron and reduced cellular iron requirements. Limnol. Oceanogr. 56(6), 1983-2002. https://doi.org/10.4319/lo.2011.56.6.1983

Tagliabue, A., Bopp, L., Aumont, O., 2009. Evaluating the importance of atmospheric and sedimentary iron sources to Southern Ocean biogeochemistry. Geophys. Res. Lett. 36(13). https://doi.org/10.1029/2009GL038914

Twining, B.S., Baines, S.B., Fisher, N.S., 2004. Element stoichiometries of individual plankton cells collected during the Southern Ocean Iron Experiment (SOFeX). Limnol. Oceanogr. 49(6), pp.2115-2128. https://doi.org/10.4319/lo.2004.49.6.2115

Wang, S., Moore, J.K., 2011. Incorporating *Phaeocystis* into a Southern Ocean ecosystem model. J. Geophys. Res. Oceans 116, C01019. https://doi.org/10.1029/2009JC005817

Zillman, J.W., 1972. A study of some aspects of the radiation and heat budgets of the southern hemisphere oceans. Bureau of Meteorology, Meteor. Stud. 26, 562

List of Figures

from the surface to 80 m which corresponds to 1% surface irradiance level. The presence of simulated sea ice is indicated (grey shading).

Figure 4: Seasonal budgets for A) nitrate-nitrogen, B) silicate, and C) dissolved iron (dFe) constructed from the Ross Sea base case simulation. Values shown for the state variables represent the contributions of each to the total nutrient pool. Values on the arrows indicate the transfer between pools. Only significant values for the nutrient pools are shown, which are defined as >1 mmol N m^{-2}, >0.5 mmol SiO_4 m^{-2}, and >1 nmol dFe m^{-2}. The values for transfers between pools are given as: m-millimoles (10^{-3}), μ-micromoles (10^{-6}), n-nanomoles (10^{-9}).

Figure 5: Simulated time evolution of surface A) particulate organic carbon (POC), B) *P. antarctica* POC and C) diatom POC obtained for input of sea ice-derived dFe that is distributed over 30 (black line), 10 (dark grey line) and 1 m (light grey line). Surface POC is calculated using total phytoplankton (TP, solid line), *P. antarctica* (PA: solitary cells and colonies, blue dash-dot line), and diatoms (D, green dashed lines). Observed values (circles) are from field measurements made in the Ross Sea (Smith et al., 2000).

Figure 6: Simulated time evolution of surface A) particulate organic carbon (POC), B) total phytoplankton POC, C) diatom POC, and D) *P. antarctica* POC obtained with mid-water inputs of dFe at 5-day (black line) and 90-day intervals (grey line) and distributed between the surface and 100 m. Surface POC is obtained for total phytoplankton (TP, solid line), *P. antarctica* (PA: solitary cells and colonies, blue dash-dot lines), and

diatoms (D, green dashed lines). Observed values (circles) are from field measurements made in the Ross Sea (Smith et al., 2000).

Figure 7: Simulated time evolution of surface A) particulate organic carbon (POC), B) total phytoplankton POC, C) diatom POC, and D) *P. antarctica* POC obtained with inputs of dissolved iron from sediments resuspended from the seafloor at 550 m (sf, grey lines) and a shallow bank at 300 m (sb, black lines). Surface POC is obtained for total phytoplankton (TP, solid lines), *P. antarctica* (PA: solitary cells and colonies, dash-dot lines), and diatoms (D, dashed lines). Observed values (circles) are from field measurements made in the Ross Sea (Smith et al., 2000).

Figure 8: Simulated time evolution of surface A) particulate organic carbon (POC), B) total phytoplankton POC, C) diatom POC, and D) *P. antarctica* POC obtained with inputs of dissolved iron from MW sources at 90-day intervals distributed between the surface and 100 m with (si, black lines) and without (grey lines) sea ice cover. Surface POC is obtained for total phytoplankton (TP, solid lines), *P. antarctica* (PA: solitary cells and colonies, dash-dot lines), and diatoms (D, dashed lines). Observed values (circles) are from field measurements made in the Ross Sea (Smith et al., 2000).

Figure 9: Simulated time evolution of surface particulate organic carbon (POC) for total phytoplankton (A, D), *P. antarctica* POC (B, E) and diatom POC (C, F) obtained with dissolved iron (dFe) inputs from the seafloor (sf) and shallow bank (sb) with (si, grey lines) and without (black lines) sea ice cover. The shadow bank inputs (sb, dashed lines)

provide dFe between 300 m and the bottom and sea floor inputs (sf, solid lines) provide dFe between 550 m and the bottom. Surface POC is obtained for total phytoplankton (TP), *P. antarctica* (PA: solitary cells and colonies), and diatoms (D). Observed values (circles) are from field measurements made in the Ross Sea (Smith et al., 2000).

Figure 10: Simulated depth-time distribution of dissolved iron concentration with inputs from iron-rich mid-water (left column), suspension of sediment from the seafloor at 550 m (middle column) and shallow banks at 300 m (right column). The simulations were done with (upper row) and without sea ice (lower row).

Figure 11: A) Contribution of dissolved iron (dFe) sources to total water column dFe concentration for the base case simulation as the percent of dFe in the surface waters (solid black line), middle water column (dotted black line) and bottom water column (dashed light grey line) and the percent dFe associated with total phytoplankton (dFe_{TP}, solid black line), diatoms ($dFe_{Diatoms}$, green dotted dashed line), *P.antarctica* solitary cells (dFe_{PA_sc}, blue dashed line) and colonies (dFe_{PA_c}, blue solid line). B) Time-depth distribution of dFe showing surface depletion by phytoplankton uptake and inputs from sea ice melt and sediment resuspension. The presence of sea ice is indicated (grey bar).

Figure 12: Conceptual model of environmental interactions that control phytoplankton blooms in the Ross sea. Surface light and nutrient inputs, especially dissolved iron (dFe) inputs from the deep-water winter reserve and melting sea ice, stimulate a *P. antarctica* bloom in early spring. Inputs of dFe via mid-water column supply sources (horizontal

and vertical mesoscale eddies and MCDW inputs) and resuspension of bottom sediments maintain the bloom and allow the transition to a diatom-dominated bloom in the latter part of the growing season.

List of Tables

Table 1: Summary of Ross Sea biogeochemical model simulations. The simulations are designed to evaluate the dissolved iron (dFe) inputs provided by melting sea ice, mid-water input (MW) and sediment resuspension on *P. antarctica* and diatom growth. The dFe source, concentration (nM), depth of influence (m), and time scale of input (per day) are given for each simulation. The dFe concentration from sea ice (dFe_{MaxVar}) varies with time following equation 29. Multiple depths of influence are denoted by parentheses. Simulations included sea ice cover, except as noted. Specifics of individual simulations are provided in the text.

Table 2: Mean daily net primary production (mmol C m^{-2} d^{-1}) of diatoms, *P. antarctica* solitary cells and colonies, and total phytoplankton obtained from simulations with and without sea ice cover and different sources of dissolved iron.

Table 3: Iron demand of diatoms, *P. antarctica* solitary cells and colonies, and total phytoplankton calculated from simulations with and without sea ice cover and different sources of dissolved iron (dFe). Method 1 is based on Kustka et al. (2015) and uses net production (Table 2) multiplied by the average Fe:C ratio (Table 4). Method 2 is based on the daily seasonal dFe uptake obtained for each simulation (supplementary document

B). Recycled dFe is the fraction of loss from phytoplankton mortality, zooplankton grazing and detrital decomposition that is remineralized relative to the total uptake of dFe by diatoms, *P. antarctica* solitary cells and colonies.

Table 4: Average Fe:C ratios (μmol Fe:mol C) of diatoms, *P.antarctica* solitary cells and colonies, and total phytoplankton calculated from simulations with and without sea ice cover and different sources of dFe. The Fe:C ratio for each phytoplankton component is calculated using the phytoplankton associated dFe and phytoplankton biomass.

Evaluation of Iron Sources in the Ross Sea, by Salmon, Hofmann, Dinniman, Smith

3 to 5 bullet points (maximum 85 characters, including spaces, per bullet point).

Highlights

- Control of Ross Sea phytoplankton by dFe was simulated with a one-dimensional model
- Input of dFe from sea ice melt initiates *Phaeocystis antarctica* blooms in early spring
- Resuspension of iron-rich sediment supports phytoplankton growth near shallow banks
- Mid- and deep-water dFe sources support diatom blooms following *P. antarctica* blooms
- *P. antarctica* contributes more chlorophyll but less POC than do diatoms